



A dual-acting 5-HT₆ receptor inverse agonist/MAO-B inhibitor displays glioprotective and pro-cognitive properties

Vittorio Canale^a, Katarzyna Grychowska^a, Rafał Kurczab^b, Mateusz Ryng^b, Abdul Raheem Keeri^a, Grzegorz Satała^b, Agnieszka Olejarz-Maciej^c, Paulina Koczurkiewicz^d, Marcin Drop^a, Klaudia Blicharz^a, Kamil Piska^d, Elżbieta Pękala^d, Paulina Janiszewska^e, Martyna Krawczyk^f, Maria Walczak^e, Severine Chaumont-Dubel^g, Andrzej J. Bojarski^b, Philippe Marin^g, Piotr Popik^f, Paweł Zajdel^{a,*}

^a Jagiellonian University Medical College, Department of Medicinal Chemistry, 9 Medyczna Str., 30-688, Kraków, Poland

^b Maj Institute of Pharmacology, Polish Academy of Sciences, Department of Medicinal Chemistry, 12 Smętna Str., 31-324, Kraków, Poland

^c Jagiellonian University Medical College, Department of Technology and Biotechnology of Drugs, 9 Medyczna Str., 30-688, Kraków, Poland

^d Jagiellonian University Medical College, Department of Pharmaceutical Biochemistry, 9 Medyczna Str., 30-688, Kraków, Poland

^e Jagiellonian University Medical College, Department of Toxicology, 9 Medyczna Str., 30-688, Kraków, Poland

^f Maj Institute of Pharmacology, Polish Academy of Sciences, Department of New Drug Development, 12 Smętna Str., 31-324, Kraków, Poland

^g Institut de Génétique Fonctionnelle, Université de Montpellier, CNRS INSERM, 34094, Montpellier, France

ARTICLE INFO

Article history:

Received 8 July 2020

Received in revised form

3 August 2020

Accepted 15 August 2020

Available online 22 August 2020

Keywords:

Neurodegenerative disorders

Alzheimer's disease

MAO-B inhibitors

5-HT₆R antagonists

Multi-target directed ligands

Constitutive activity

Glia

Cognition

ABSTRACT

The complex etiology of Alzheimer's disease has initiated a quest for multi-target ligands to address the multifactorial causes of this neurodegenerative disorder. In this context, we designed dual-acting 5-HT₆ receptor (5-HT₆R) antagonists/MAO-B inhibitors using pharmacophore hybridization strategy. Our approach involved linking privileged scaffolds of 5-HT₆R with aryloxy fragments derived from reversible and irreversible MAO-B inhibitors. The study identified compound **48** that acts as an inverse agonist of 5-HT₆R at G_s signaling and an irreversible MAO-B inhibitor. Compound **48** showed moderate metabolic stability in rat microsomal assay, artificial membrane permeability, no hepatotoxicity, and it was well distributed to the brain. Additionally, **48** showed glioprotective properties in a model of cultured astrocytes using 6-OHDA as the cytotoxic agent. Finally, compound **48** (MED = 1 mg/kg, *p.o.*) fully reversed memory deficits in the NOR task induced by scopolamine in rats. A better understanding of effects exerted by dual-acting 5-HT₆R/MAO-B modulators may impact the future development of neurodegenerative-directed treatment strategies.

© 2020 Elsevier Masson SAS. All rights reserved.

1. Introduction

Neurodegenerative diseases are chronic conditions which involve progressive loss of neuronal and glial cells, demyelination, and overall structural and functional brain deficits. Among these diseases, Alzheimer's disease (AD) is the most common disorder characterized by continuous deterioration of cognitive functions, resulting in complete disability in the elderly life. The increasing

prevalence of AD, together with the lack of effective therapy that could slow down the progression of the disease, makes it one of the biggest global health challenges [1].

Unfortunately, therapeutically useful disease-modifying and symptomatic drug candidates for AD developed in the two past decades have shown disappointing results [2–4]. Nonetheless, our understanding of G protein-coupled receptors (GPCRs) signaling networks, and compensatory mechanisms related to enzyme inhibition [5] and disease pathology steadily grew, thereby opening new opportunities for drug discovery. In particular, more focus was given to develop new strategies using multi-target directed ligands (MTDL) to address the etiology and symptoms of such a complex

* Corresponding author. Jagiellonian University Medical College, Department of Medicinal Chemistry, Poland.

E-mail address: pawel.zajdel@uj.edu.pl (P. Zajdel).

and debilitating disease. Accumulating evidence revealed that connecting and/or merging structural fragments, which simultaneously affect different biological targets, is one of the most promising areas of anti-AD drug development [6,7]. Several MTDLs have been reported, with the most prominent examples being dual enzymatic inhibition of acetylcholinesterase (AChE) and glycogen synthase kinase (GSK-3 β) [8], inhibition of AChE and monoamine oxidase B (MAO-B) [9,10] and inhibition of β -secretase (BACE-1) and GSK-3 β [11]. The MTDL strategy is further completed with GPCRs dual-acting compounds as 5-HT₆/D₃ and 5-HT_{2A}/5-HT₆ receptor antagonists [12–15] as well as 5-HT₄R agonist/5-HT₆R antagonist [16]. However, simultaneous targeting of enzyme and receptor activities constitutes a more challenging area. This stems from limitations in finding common binding modes and structural features for targets with different location and structural requirements [17]. Among examples of such an approach, the dual-acting compounds described thus far include AChE inhibitors and NMDA receptor antagonists [18], AChE and histamine H₃ receptor (H₃R) antagonists [19], AChE inhibitors and sigma σ_1 receptor ligands [20], AChE inhibitors and serotonin 5-HT₄R agonists [21] or AChE inhibitors and 5-HT₆R antagonists [22].

Serotonin type 6 receptor (5-HT₆R) is a GPCR which has emerged as a promising target for the treatment of pro-cognitive deficits of neurodegenerative and psychiatric disorders. It is almost exclusively expressed in the central nervous system (CNS), particularly in brain regions involved in cognitive processes, i.e., prefrontal cortex, hippocampus and striatum. 5-HT₆R is primarily located in the cilia of neurons which are sensory organelles that participate in neurodevelopment and neuronal differentiation [23–26].

Pharmacological blockade of 5-HT₆R, located on GABA-ergic and glutamatergic neurons, increases cholinergic transmission [27,28]. Consequently, 5-HT₆R antagonists show beneficial effects on cognition, as shown by a various preclinical studies and preliminary clinical studies [29–31] that revealed pro-cognitive effects in humans [32]. However, phase III clinical trials for these compounds showed disappointing results.

The recent findings on the elevated level of MAO-B in AD brains, corroborated by data showing a MAO-B-dependent control of amyloid- β production in neurons *via* γ -secretase, suggest a role of MAO-B in AD [33]. MAO-B is mainly found in the outer membrane of the mitochondria in non-neuronal cells, such as glial cells [34,35]. It is a membrane-bound FAD-containing enzyme, involved in the degradation of monoamines, including dopamine. It has been demonstrated that the production of reactive oxygen species, resulting from the activity of MAO-B, increases with age. Furthermore, an elevated level of this enzyme has been found in astrocytes and pyramidal neurons of AD brains [33,36]. Based on these observations, MAO-B inhibitors have been investigated as potential neuroprotective agents for the treatment of neurodegenerative disorders [37].

To determine how to target two distinct proteins with different pharmacophore requirements, we analyzed the binding mode in the 5-HT₆R homology model and sought opportunities to target MAO-B catalytic center using induced fit-docking (IFD) and quantum mechanics/molecular mechanics (QM/MM) calculations. This prospective *in silico* analysis, guided the design and synthesis of a new series of hybrid compounds obtained by linking pharmacophore fragments of 5-HT₆R antagonists with molecular frameworks of known MAO-B inhibitors in a unique molecular entity (Fig. 1). Structural modifications comprised functionalization of N¹ atom of (indol-4-yl)piperazine with 3-chlorobenzyl and benzenesulfonyl moieties in the 5-HT₆R-aiming substructure and diversification of aryloxy fragments derived from reversible and irreversible MAO-B inhibitors, both connected *via* an alkylene spacer of different

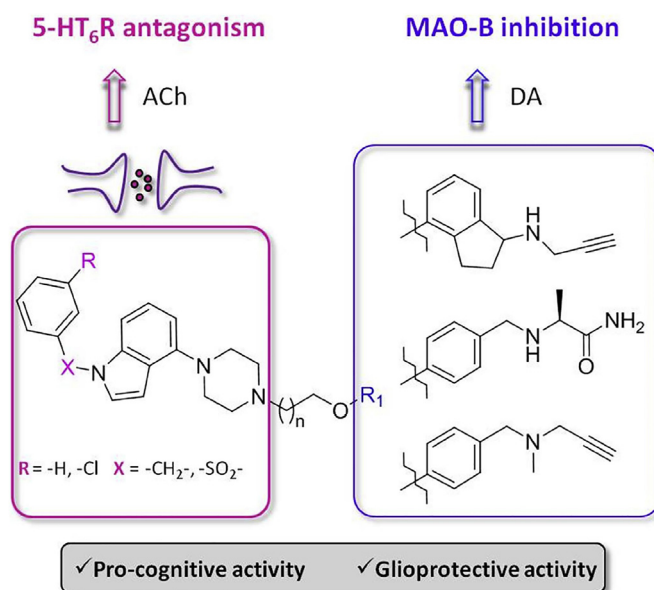


Fig. 1. The design strategy of dual-acting 5-HT₆R/MAO-B modulators.

length. Here, we evaluated the structure-activity relationship (SAR) within novel dual-acting compounds exhibiting inhibitory activity for 5-HT₆R and MAO-B. We selected a lead compound (compound 48), for which we performed more detailed mechanistic studies. We assessed its action on both targets and examined its distribution to the CNS following peripheral administration. Finally, we showed that this dual 5-HT₆R inverse agonist/MAO-B inhibitor protects astrocytes against 6-hydroxydopamine (6-OHDA)-induced toxicity and reverses scopolamine-induced cognitive impairment in the novel object recognition (NOR) task in rats.

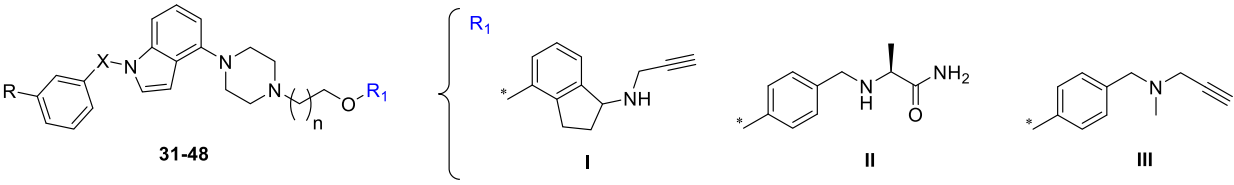
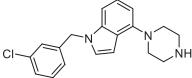
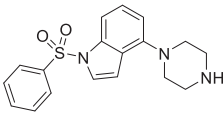
2. Chemistry

The designed compounds were synthesized in two stages. First, the respective building blocks, namely functionalized (indol-4-yl) piperazine **5** and **6** (Scheme 1A) and alkylating agents **9–17** (Scheme 1B), were obtained using parallel synthetic routes. Commercially available 4-bromoindole **1** was subjected to Buchwald-Hartwig *N*-arylation to yield 4-(4-Boc-piperazin-1-yl) indole. Simple heating of the obtained product in ethanol at 150 °C using microwave irradiation eliminated Boc protecting function and provided 1*H*-indole intermediate **2**. This was subsequently reacted with 3-chlorobenzyl bromide or benzenesulfonyl chloride, in the presence of phosphazene base (BTPP) to afford indoles **3** and **4**. Treatment of the latter compounds with TFA furnished secondary amines **5** and **6**, respectively.

In parallel, commercially available phenols **7** and **8** were reacted with an excess of different α,ω -dibromoalkane in biphasic conditions, to give respective alkylating agents **9–17** (Scheme 2). Intermediates **9–17** were subsequently combined with secondary amines **5** and **6**, yielding derivatives **18–30**, by stirring in acetone at 60 °C, in the biphasic system, for 16 h.

Final compounds **31–48** were obtained by reductive amination, using sodium triacetoxyborohydride (STAB) in THF for primary amines or STAB in CH₂Cl₂ for secondary amines.

Table 1Affinity for 5-HT₆R and potency for MAO-B inhibition of synthesized compounds **31–48** and reference 5-HT₆R ligands and MAO-B inhibitors.

						
Compd	R	X	N	R ₁	K _i [nM] ^a h5-HT ₆ R	IC ₅₀ [nM] ^b and (%inh) ^c hMAO-B
31	Cl	CH ₂	1	I	100	> 1000 (35)
32	Cl	CH ₂	2	I	77	> 1000 (31)
33	Cl	CH ₂	3	I	113	270 ± 43 (100)
34	Cl	CH ₂	4	I	223	460 ± 51 (80)
35	Cl	CH ₂	5	I	259	> 1000 (34)
36	H	SO ₂	3	I	50	> 1000 (44)
37	H	SO ₂	4	I	51	163 ± 25 (90)
38	Cl	CH ₂	2	II	158	> 1000 (47)
39	Cl	CH ₂	3	II	162	> 1000 (24)
40	Cl	CH ₂	4	II	232	> 1000 (43)
41	Cl	CH ₂	5	II	340	> 1000 (23)
42	H	SO ₂	3	II	68	> 1000 (20)
43	H	SO ₂	4	II	65	> 1000 (17)
44	Cl	CH ₂	3	III	195	323 ± 42 (85)
45	Cl	CH ₂	4	III	140	30 ± 2 (100)
46	Cl	CH ₂	5	III	137	> 1000 (32)
47	H	SO ₂	3	III	54	> 1000 (51)
48	H	SO ₂	4	III	38	154 ± 19 (91)
A					7	(3)
B					0.3	(3)
Intepirdine^d					1.4	N.T. ^e
Rasagiline					N.T. ^e	15.4 ± 0.6 (100)
Safinamide					N.T. ^e	7 ± 1.2 (100)

^a Mean K_i values (SEM ± 15%) based on three independent binding experiments^b IC₅₀ ± SEMs values were determined using rasagiline [1 μM] as positive control^c % of inhibition of control (rasagiline, 1 μM) at 1 μM^d Data taken from [30]^e not tested.

3. Results and discussion

3.1. Structure-activity relationship studies

The molecular framework of the dual-acting derivatives was based on the pharmacophore hybridization strategy supported with prospective *in silico* analysis of homology model of 5-HT₆R and crystal structure of MAO-B. The strategy involved connecting pharmacophore structures of known selective 5-HT₆R antagonists and MAO-B inhibitors in a single molecule. The selection of phenylsulfonyl-4-(piperazin-1-yl)-1H-indole (**A**) and N-3-chlorobenzyl-4-(piperazin-1-yl)indole (**B**) as 5-HT₆R-targeting fragments, was based on literature survey and unpublished data. Our results indicated that compounds containing unsubstituted phenylsulfonyl moiety are highly potent 5-HT₆R ligands, whereas their benzyl analogs require substitution with a chlorine atom in the *meta* position [38].

To achieve inhibition of MAO-B activity, aryloxy fragments

derived from rasagiline, safinamide and pargyline were linked to the 5-HT₆R pharmacophore *via* different length alkylene linker. Because the molecular framework of the designed hybrids is different from that of classical MAO-B inhibitors (they are very long, with two basic centers and a flexible alkylene linker), the possibility of interaction with the catalytic domain of MAO-B was supported by *in silico* experiments. Indeed, molecular dynamics studies indicated the existence of two entrance channels to the MAO-B binding site for inhibitors (more details in SI), i.e., membrane accessed (A), and solvent accessed (B) [39]. An analysis of ligand-enzyme complexes for MAO-B crystals showed that entrance A is closed for several compounds, whereas entrance B forms a narrow channel. IFD for the designed compounds provided a static view of the conformation of the enzyme, showing that the only way to enter the catalytic center is through entrance B, which is devoid of significant steric hindrances. It should be emphasized here that such large compounds would be unable to enter the catalytic MAO-B through entrance A, because it would be sterically disturbed by

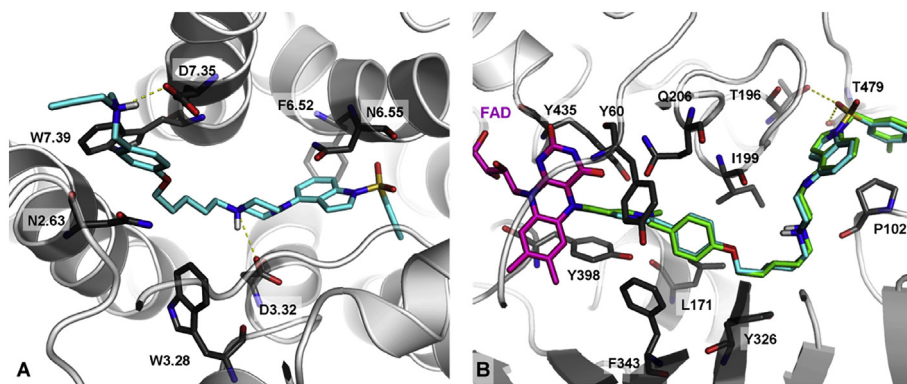


Fig. 2. The binding mode of **48** (cyan) in 5-HT₆R (A), and comparison of binding modes of **45** (green) and **48** (cyan) in the MAO-B catalytic site (B). (For interpretation of the references to color in this figure legend, the reader is referred to the Web version of this article.)

Table 2

Binding data of selected compound **48** and intepirdine for 5-HT₆, 5-HT_{1A}, 5-HT_{2A}, 5-HT₇, and D₂Rs and inhibitory activity (IC₅₀ values) for MAO-B and MAO-A.

Compd	K _i [nM] ^a					IC ₅₀ ^b	
	5-HT ₆	5-HT _{1A}	5-HT _{2A}	5-HT ₇	D ₂	MAO-B	MAO-A
48	38	684	420	7996	813	154	1037
Intepirdine ^c	1.4	2370	26	14 230	997	NT ^d	NT ^d

^a Mean K_i values (SEM ±25%) based on three independent binding experiments.

^b IC₅₀ ± SEMs values was determined using rasagiline [1 μM] or clorgyline [1 μM] as positive control for MAO-B and MAO-A, respectively.

^c Data taken from [30].

^d Not Tested.

the mitochondrial membrane.

The newly synthesized compounds **31–48** showed moderate affinity for 5-HT₆R in [³H]-LSD binding experiments and low-to-high inhibitory potency for MAO-B, with IC₅₀ values ranging from 30 to >1000 nM as assessed using the fluorimetric method (Table 1).

Generally, linking 5-HT₆R pharmacophores with MAO-B-targeting fragments decreased affinity for 5-HT₆R when compared with the parent compounds **A** and **B**. However, this modification did not totally preclude the interaction of the obtained derivatives with the binding cavity of 5-HT₆R (K_i = 38–340 nM). Compounds bearing N¹-sulfonyl moiety were more potent 5-HT₆R ligands than their congeners with methylene bridge, regardless of the length of the alkylene linker and the kind of MAO-B fragment (**34** vs **37** and **44** vs **47**). Analysis of the obtained ligand-receptor complexes for compound **48** exhibiting the highest affinity for 5-HT₆R (Fig. 2A), showed that the protonated piperazine fragment

Table 3

The antagonist property of compound **48** and intepirdine in 1321N1 cells and their functional activity at 5-HT₆R-dependent Gs signaling in NG108-15-based model.

Compd	K _b [nM] ^a	IC ₅₀ [nM] ^b	Functional profile
	5-HT ₆		
48	6 ± 1	860 ± 0.68	Inverse Agonist
Intepirdine	1.3 ± 0.2	97 ± 0.21	Inverse Agonist

^a Mean K_b ± SEMs of values obtained in three independent experiments in 1321N1 cells.

^b Mean IC₅₀ ± SEMs of values obtained in three independent experiments in NG108-15 cells.

formed a salt bridge with D3.32, the indole ring was positioned in the conserved aromatic cluster of F6.51 and F6.52, and the terminal phenyl ring was accommodated in a hydrophobic cavity formed by transmembrane domains 3–5 and extracellular loop 2. It should be noted that the indole and phenyl rings form an angle of approximately 90°, resulting from the tetrahedral geometry (sp³) of sulfonyl linkers. In turn, the propargyl moiety at the aryloxy fragment was directed toward the extracellular part of the receptor, with the phenyl ring positioned between N2.63 and W7.39, and protonated the N-methyl-propargylamine forming a salt bridge with D7.35.

Exploration of SAR toward MAO-B revealed that sulfonamide derivatives were less preferred for the interaction with the enzymatic target than their benzyl analogs (**33** vs **36**, **40** vs **43**, and **44** vs **47**). More detailed analysis of the aryloxy terminal fragment, indicated that compounds **38–43** bearing safinamide-derived alaninamide moiety, showed low inhibitory potency against enzyme. On the other hand, the presence of propargyl- and N-methyl-propargylamine (originated from rasagiline and pargyline, respectively) increased the inhibitory effect (31–100% inhibition), thus highlighting the pivotal role of covalent bond formation of compounds **33**, **37**, **45** and **48** with FAD cofactor in the enzymatic target. With regard to the length of the alkylene chain, five methylene linked hybriides (**37**, **45**, **48**) exhibited the highest inhibition activity for MAO-B. This observation was further confirmed by *in silico* studies. The binding modes of the most potent MAO-B inhibitors **45** and **48** (Fig. 2B) were coherent and showed accommodation of the molecules in an “aromatic cage” formed by Y435, Y398, Y60, and F343, which are considered crucial in the ligand positioning for the reaction with FAD [40–42]. Additionally, the hydrogen bond between the side chain of Q206 and the nitrogen atom of the propargyl functional group seems to play a role in placing this fragment in an optimal position [42].

3.2. Determination of selectivity profile for compound **48**

The SAR analysis allowed to identify the most potent dual-acting compound **48** possessing a phenylsulfonyl moiety at (indol-4-yl) piperazine scaffold in tandem with aryloxy fragments derived from pargyline, connected via a four methylene spacer (K_i 5-HT₆R = 38 nM, IC₅₀ MAO-B = 154 nM). Subsequently, compound **48** was profiled *in vitro* for selectivity over structurally-related GPCRs and MAO-A enzyme isoform (Table 2).

Compound **48** showed moderate to high selectivity over 5-HT_{1A}, 5-HT_{2A}, 5-HT₇, and D₂ receptors. Although it contains aryloxy fragments derived from pargyline (a known non-selective MAO inhibitor), it showed moderate inhibitory activity toward the MAO-A enzyme isoform, thus reducing the possibility to elicit

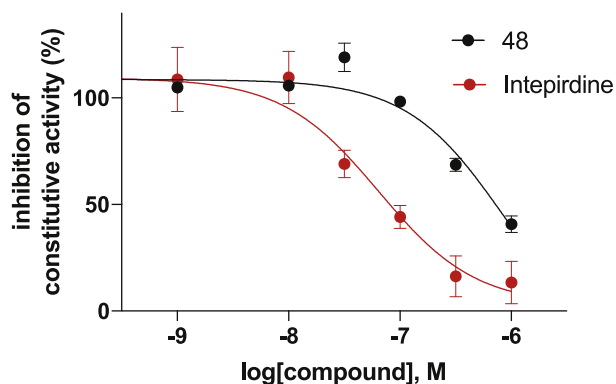


Fig. 3. Influence of compound **48** and intepirdine on basal cAMP production in NG108-15 cells transiently expressing 5-HT₆R. Data are the means \pm SEM of the values obtained in three independent experiments performed in quadruplicate in different sets of cultured cells. *** $p < 0.001$ vs. vehicle (ANOVA followed by Student–Newman–Keuls test).

cardiovascular side effects (i.e., hypertensive crisis).

To exclude potential risks related to undesired cardiovascular or CNS side effects, the affinity of compound **48** for selected “off-target” receptors was assessed by Eurofins Scientific. The tested compound displayed low affinity for α_{1A} adrenoreceptor (% inhibition at 1 μ M = 37%) and did not bind to β_1 adrenoreceptor (% inhibition at 1 μ M = 5%), H₁ histaminic receptor (% inhibition at

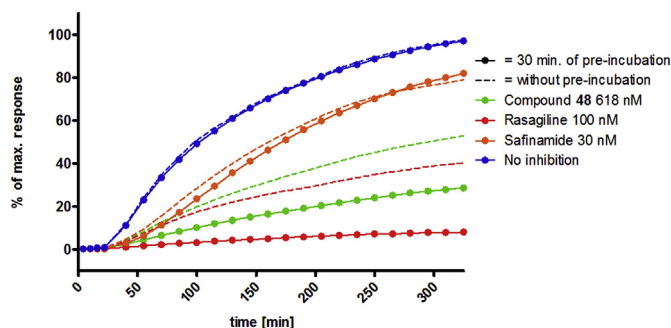


Fig. 4. Reactivation of MAO-B activity upon blockade with compound **48** and reference inhibitors used at a concentrations corresponding to their IC₈₀ values in the presence of the substrate p-tyramine. All compounds were tested with 30 min of pre-incubation (rings) and without pre-incubation (lines). Data are presented as mean values from two independent experiments run in duplicate. The results were normalized to the effect induced by 1 mM of p-tyramine (100% value) and solvent (0% value) in the last measurement of the experiment.

1 μ M = 13%) and M₁ muscarinic receptor (% inhibition at 1 μ M = 4%).

3.3. Impact of compound **48** on 5-HT₆R-operated signaling and on MAO-B activity

The impact of compound **48** on adenylate cyclase activity was first examined in 1321N1 cells expressing 5-HT₆R and treated with 5-carboxamidotryptamine (5-CT), a 5-HT₆R agonist. Compound **48** behaved as a potent antagonist of 5-HT₆R in this cellular assay (K_b = 6 nM, Table 3).

The high level of constitutive activity of 5-HT₆R, defined as the ability of the receptor to adopt an active conformation able to transduce signal in the absence of an agonist, has been demonstrated in both *in vitro* and *ex vivo* models [43,44]. This property

opens up the possibility to classify 5-HT₆R ligands as inverse agonists or neutral antagonists [30,45].

Hence, the ability of compound **48** to modulate agonist-independent 5-HT₆R-operated Gs signaling was tested in NG108-15 cells transiently expressing 5-HT₆R, a cellular model in which the receptor displays high constitutive activity [44,46]. We found that compound **48** decreased basal cAMP level in a concentration-dependent manner (IC_{50} = 860 ± 0.68 nM) but its apparent affinity was much lower than that of the prototypic 5-HT₆R inverse agonist intepirdine (Table 3, Fig. 3).

To investigate the inhibitory mechanism of compound **48** on hMAO-B, time-dependent inhibition studies were performed using *in vitro* method. Rasagiline and safinamide, with known irreversible and reversible inhibition toward MAO-B were used as reference drugs (Fig. 4). In the case of reversible inhibitor safinamide, the competing excess of p-tyramine, used as an enzyme substrate, significantly reactivated the enzyme activity. In contrast, rasagiline, depending on the pre-incubation time used, has either slightly restored MAO-B activity or maintained only residual activity of the enzyme. A higher than expected signal for rasagiline without pre-incubation (ca. 30% reactivation) might be explained by the longer time required to create the covalently bound inhibitor-enzyme complex by irreversible inhibitors. Although compound **48** was able to restore some activity of MAO-B, the difference between the enzyme reactivation rate, obtained with and without pre-incubation, suggests that compound **48** covalently modify the enzyme.

3.4. Preliminary evaluation of ADME/Tox properties

As ligands that combine two pharmacophore fragments within a single molecule usually have physicochemical properties burdens (high molecular weight or clog P value), which might limit their bioavailability, compound **48** was subsequently evaluated for its drug-likeness in *in vitro* screening. The ability to cross the blood-brain barrier (BBB) by passive diffusion was assessed by the commonly used parallel artificial membrane permeability assay (PAMPA-BBB) [47]. Compound **48** showed an efficient permeability (Pe) value greater than 4.0 in the tested conditions, thus suggesting a high CNS penetration (Table 4). The reference drugs verapamil (Pe = 1.85×10^{-5} cm/s) and doxorubicin (not detected in the acceptor compartment) were used as positive and negative control, respectively.

Subsequently, the *in vitro* metabolic stability of compound **48** was determined using rat liver microsomes (RLMs). After 60-min incubation period, compound **48** showed an average intrinsic clearance (Cl_{int}) of 85 mL/min/kg (Table 4).

Compound **48** was also submitted to preliminary hepatotoxicity assessment using human liver cancer cell (HepG2). As revealed by the MTT assay compound **48** did not affect the viability of HepG2 cells after 24-h period (Table 4). Doxorubicine used as reference cytotoxic drug showed more than 20-fold higher cytotoxic activity (IC_{50} = 2.3 μ M).

Next, the preliminary pharmacokinetic profile of compound **48** was estimated in male Wistar rats injected with a single dose (3 mg/kg *p.o.*). Compound **48** was rapidly absorbed and was able to cross the BBB with a C_{max} value reaching 72.7 ng/mL in the brain after 30 min (T_{max}, Table 4). The molecule was eliminated very slowly from the rat body, with along half-life of ca. 28 h.

3.5. Glioprotective effects

Given the supporting role of glial cells in the CNS, protection of astrocytes might be a relevant strategy for treating neurodegenerative disorders in addition to direct action on neuronal cell

Table 4
Summary of the ADME/Tox profile evaluation for compound **48**.

Assay type	48
PAMPA permeability	$Pe = 4.84 \times 10^{-6} \text{ cm/s}^a$
Microsomal stability	$Cl_{int} = 85 \text{ mL/min/kg}^b$
Hepatotoxicity	$IC_{50} = 52.7 \text{ }\mu\text{M}^c$
Preliminary <i>in vivo</i> pharmacokinetics ^d	$C_{max} = 72.7 \text{ ng/mL}$ $T_{max} = 30 \text{ min}$

^a Measured at 100 μM initial concentration at pH 7.4 in a phosphate buffer at room temperature measured at pH 7.4 in a phosphate buffer at room temperature.

^b Determined at a protein concentration of 0.4 mg/mL in RLM assay.

^c Concentration that inhibits 50% of HepG2 cell growth, when treated with tested compounds for 24-h period; IC_{50} was obtained from three independent experiments, using GraphPad Prism software.

^d Measured after *p.o.* administration of dose 3 mg/kg.

functions or survival [48]. We thus explored the glioprotective effects of compound **48** in a model of cultured astrocytes (C8-D1A astrocytes) exposed to the neurotoxin 6-OHDA. 6-OHDA-induced cell death is attributed to the oxidative damage by reactive oxygen species (ROS) derived from 6-OHDA autooxidation or possible direct effect of 6-OHDA on the mitochondrial respiratory chain complex [49].

As revealed by the MTT assay (which assesses mitochondrial metabolism), compound **48** did not induce significant toxicity in C8-D1A astrocyte cultures at concentrations up to 25 μM but protected C8-D1A astrocytes against 6-OHDA-induced cytotoxicity (Fig. 5A). These observations were confirmed in lactate dehydrogenase (LDH) assay, which assesses cell membrane integrity (Fig. 5B). Notably, intepirdine exhibited no glioprotective properties [13]. Similarly, although neuroprotective activity of selegiline was established in several *in vitro* models [50], this irreversible MAO-B inhibitor did not reduce gliotoxicity induced by 6-OHDA in both cell-based assays (Fig. 5A and B). These findings suggest that blockade of MAO-B alone is not sufficient to protect C8-D1A astrocytes against 6-OHDA toxicity, and that the glioprotective effect of compound **48** results either from 5-HT₆ receptor antagonist/inverse agonist activity or from its dual inhibitory activities on 5-HT₆R and MAO-B.

3.6. Pro-cognitive properties

Given the interesting multipotent activity of compound **48**, its ability to rescue cognitive deficit induced by scopolamine (SCOP) in rats was then investigated using the NOR test. Scopolamine administration (1.25 mg/kg, *p.o.*) abolished the ability of rats to discriminate between novel and familiar objects when compared to the vehicle-treated animals. These deficits were significantly reversed by *p.o.* administration of compound **48** at the doses of 1 and 3 mg/kg (Fig. 6).

4. Conclusions

Using the strategy of dual-acting compounds, we designed and synthesized a series of hybrids that combine a (indol-4-yl)-piperazine fragment—a well-established core of 5-HT₆R antagonists—with frameworks of known MAO-B inhibitors, connected through an alkylene linker. As revealed by *in silico* studies, despite the size of the molecular framework, designed derivatives could enter the binding site of MAO-B by a solvent accessed channel B, which is devoid of significant steric hindrances. In agreement with the design rationale, the majority of novel hybrid compounds showed affinity for 5-HT₆R and inhibitory activity for the enzyme target. The study identified compound **48**, a dual 5-HT₆R/MAO-B modulator, which behaved as an inverse agonist of 5-HT₆R at the G_s

signaling pathway and an irreversible MAO-B inhibitor. Besides showing the most efficient combination of 5-HT₆R modulation and MAO-B inhibitory activity, compound **48** was metabolically stable and brain penetrant. Moreover, compound **48** reduced the gliotoxic effect of 6-OHDA in C8-D1A astrocytes in two complementary assays (MTT and LDH) assessing cell survival. Importantly, this effect was not observed after treatment with intepirdine (5-HT₆R antagonist) and MAO-B inhibitor selegiline. Finally, compound **48** also reversed cognitive decline induced by scopolamine in the NOR test. These properties highlight **48** as an original example of dual 5-HT₆R/MAO-B modulator and as an interesting prototype in the development of new treatment strategies for AD.

5. Experimental procedures

5.1. Chemistry

5.1.1. General methods

The synthesis was carried out at ambient temperature, unless indicated otherwise. Organic solvents (from Aldrich and Chempur) were of reagent grade and were used without purification. All reagents (Sigma-Aldrich, Fluorochem, Across and TCI) were of the highest purity. Column chromatography was performed using silica gel Merck 60 (70–230 mesh ASTM).

Mass spectra were recorded on a UPLC-MS/MS system consisted of a Waters ACQUITY® UPLC® (Waters Corporation, Milford, MA, USA) coupled to a Waters TQD mass spectrometer (electrospray ionization mode ESI-tandem quadrupole). Chromatographic separations were carried out using the Acquity UPLC BEH (bridged ethyl hybrid) C18 column; 2.1 \times 100 mm, and 1.7 μm particle size, equipped with Acquity UPLC BEH C18 Van Guard pre-column; 2.1 \times 5 mm, and 1.7 μm particle size. The column was maintained at 40 °C, and eluted under gradient conditions from 95% to 0% of eluent A over 10 min, at a flow rate of 0.3 mL min⁻¹. Eluent A: water/formic acid (0.1%, v/v); eluent B: acetonitrile/formic acid (0.1%, v/v). Chromatograms were made using Waters e λ PDA detector. Spectra were analyzed in 200–700 nm range with 1.2 nm resolution and sampling rate 20 points/s. MS detection settings of Waters TQD mass spectrometer were as follows: source temperature 150 °C, desolvation temperature 350 °C, desolvation gas flow rate 600 L h⁻¹, cone gas flow 100 L h⁻¹, capillary potential 3.00 kV, cone potential 40 V. Nitrogen was used for both nebulizing and drying gas. The data were obtained in a scan mode ranging from 50 to 2000 *m/z* in time 1.0 s intervals. Data acquisition software was MassLynx V 4.1 (Waters). The UPLC/MS purity of all the final compounds was confirmed to be 95% or higher.

¹H NMR and ¹³C NMR spectra were obtained JOEL JNM-ECZR500 RS1 (ECZR version) at 500 and 126 MHz, respectively and are reported in ppm using deuterated solvent for calibration (CDCl₃ or DMSO-*d*₆). The *J* values are reported in Hertz (Hz), and the splitting patterns are designated as follows: br. s. (broad singlet), s (singlet), d (doublet), t (triplet), q (quartet), dd (doublet of doublets), m (multiplet).

Elemental analysis for C, H, N and S was carried out using the elemental Vario El III Elemental Analyser (Hanau, Germany). All values are given as percentages, and were within $\pm 0.4\%$ of the calculated values.

Compound **48** selected for behavioral evaluation was converted into the hydrochloride salt.

All synthetic procedures and spectroscopic data for selected final compounds are summarized below, while characterization data for all intermediates and remained final compounds are reported in the Supporting Information.

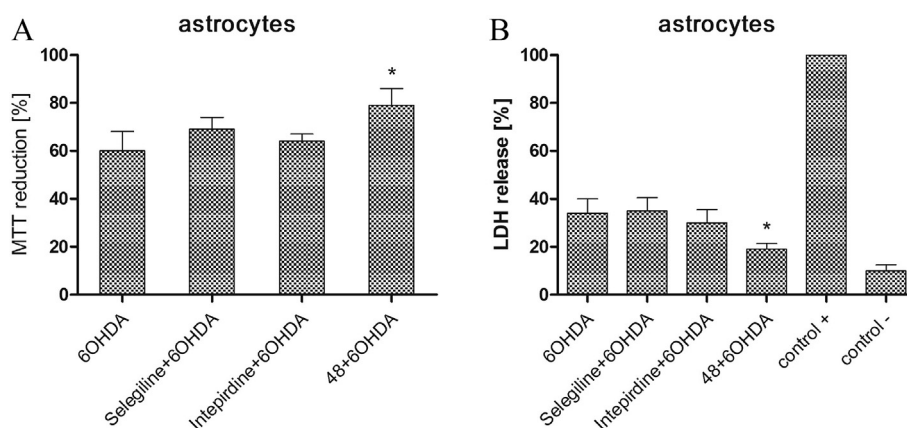


Fig. 5. Effect of selegiline, intepirdine, and **48** on 6-OHDA-induced astrocytes cytotoxicity. (A) MTT and (B) LDH assays were performed on astrocytes pre-treated with the tested compounds (0.25 μ M) for 24 h and injured by 6-OHDA (25 μ M) for the next 24-h period. $p < 0.05$ vs 6-OHDA.

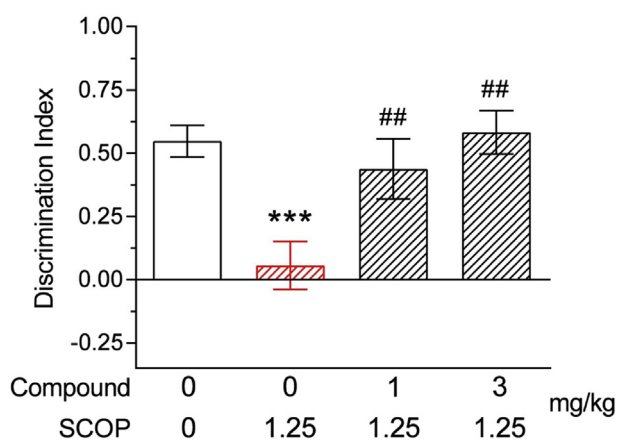


Fig. 6. Effects of compound **48** on SCOP-induced inhibition of novelty discrimination in the NOR test in rats. The data illustrated represent discrimination index (DI) and are the mean \pm standard error of the mean of $N = 6-10$ animals per group. Symbols: *** $p < 0.001$ vs vehicle-treated group; ## $p < 0.01$ vs SCOP-treated group.

5.1.2. General procedure for the *N*-arylation of *N*-Boc-4-bromoindole and selective Boc-deprotection (**2**)

N-Boc-4-bromoindole derivative (5 g, 16.88 mmol, 1 eq), Boc-piperazine (6.28 g, 33.77 mmol, 2 eq), tris(dibenzylideneacetone) dipalladium (310 mg, 0.34 mmol, 0.02 eq), BINAP (420 mg, 0.68 mmol, 0.04 eq) and NaOtBu (1.77 g, 18.38 mmol, 1.5 eq) were solubilized in toluene anhydrous (30 mL) in a 250 mL reaction flask. The flask was evacuated and back filled with argon and the reaction was left stirring at 110 $^{\circ}$ C for 5 h. Then, the mixture was diluted with AcOEt (50 mL) and filtered off on Celite pad and finally concentrated. The crude mixture was purified on silica gel using a mixture of AcOEt/Hex (1/9, v/v) as eluting system. Next, the pure intermediate (4.3 g, 10.71 mmol) was dissolved in EtOH (80 mL) and portioned in 4 seal-closed microwave reactors. Each reactor was irradiated for 2 h at 150 $^{\circ}$ C. Then, organic solvent was removed under vacuum and the resulting product (3.07 g, 95% yield) was pure enough for the next synthetic step.

5.1.3. General procedure for benzylation or sulfonylation of the *N*¹-indole moiety (**3-4**)

A solution of *tert*-butyl 4-(1*H*-indol-4-yl)piperazine-1-carboxylate (1.5 g, 4.98 mmol, 1 eq) in CH_2Cl_2 (20 mL) was cooled to 0 $^{\circ}$ C followed by addition of phosphazene base *P*₁-*t*-Bu-tris(tetramethylene) (2.27 mL, 7.47 mmol, 1.5 eq). Then, the mixture was

treated with 3-chlorobenzyl bromide (0.98 mL, 7.47 mmol, 1.5 eq) or benzenesulfonyl chloride (0.95 mL, 7.47 mmol, 1.5 eq) and stirred for 2 h at rt. After removal of organic solvents, the crude products were purified on silica gel using a mixture of AcOEt/Hex as eluting system.

5.1.4. General procedure for Boc deprotection at piperazine moiety (**5-6**)

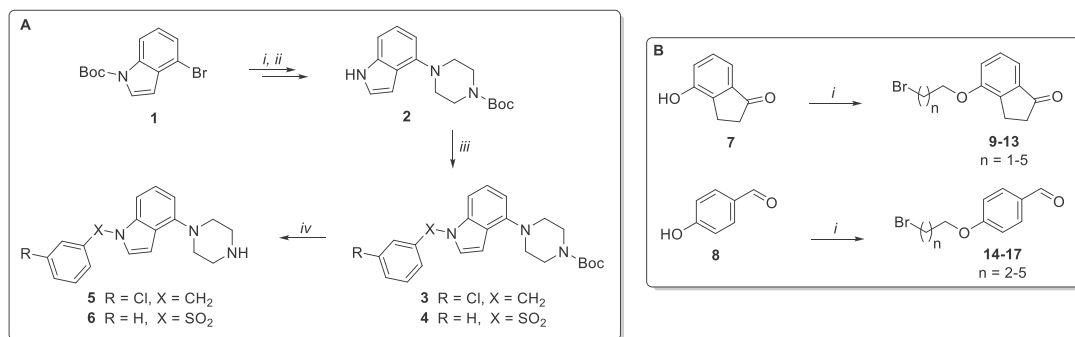
Intermediate **3** (1.45 g, 3.4 mmol) was solubilized in CH_2Cl_2 (12 mL) and cooled to 0 $^{\circ}$ C followed by addition of TFA (3 mL). The reaction mixture was stirred for 2 h at rt. Then, the reaction was diluted with CH_2Cl_2 (5 mL) and the acidic excess was carefully neutralized with cold NH_3 aqueous solution till pH = 10. The organic fraction was washed with brine (1 x), dried over anhydrous Na_2SO_4 , filtered and concentrated under vacuum. The resulting product **5** was submitted to the next step without further purification. According to the same procedure intermediate **4** was converted into secondary amine **6**.

5.1.5. General procedure for alkylation of phenols (**9-13** and **14-17**)

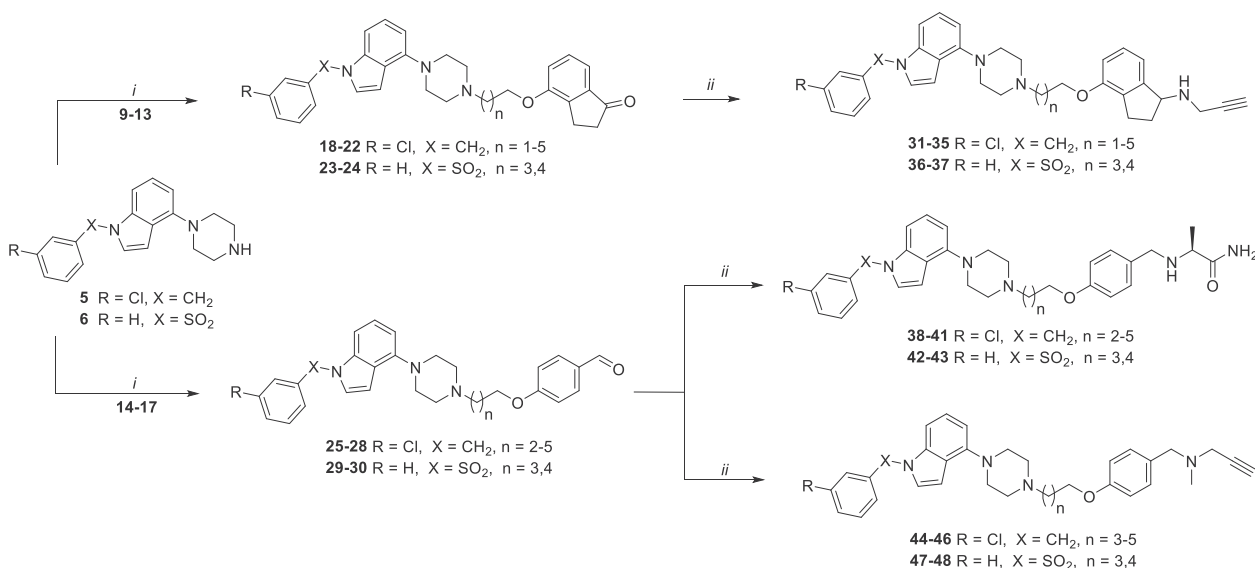
A suspension of 4-hydroxy-indanone (0.75 g, 5.06 mmol, 1 eq), freshly grinded K_2CO_3 (1.75 g, 12.66 mmol, 2.5 eq) and KOH (0.14 g, 2.53 mmol, 0.5 eq) in 15 mL of acetone. The proper di-bromoalkane (20.24 mmol, 4 eq) was slowly dropped to the reaction mixture and then left stirring at 60 $^{\circ}$ C overnight. Then, inorganic residues were filtered off, followed by removal of organic solvent under vacuum. The crude products were purified on silica gel using a mixture of AcOEt/Hex as eluting system. to obtain intermediates **9-13**. The same procedure was employed for the alkylation 4-hydroxybenzaldehyde with different di-bromoalkane to achieve intermediates **14-17**.

5.1.6. General procedure for the alkylation of *N*¹-functionalized-4-indol-piperazine (**18-30**)

1-(3-Chlorobenzyl)-4-(piperazin-1-yl)-1*H*-indole **5** (150 mg, 0.46 mmol 1 eq) and freshly grinded K_2CO_3 (190 mg 1.38 mmol, 3 eq) were suspended in 5 mL of acetone, followed by the dropwise addition of the corresponding alkylating agent **9-17** (0.55 mmol, 1.2 eq). The reaction mixture was stirred at 60 $^{\circ}$ C overnight. Then, inorganic residues were filtered off, followed by removal of organic solvent under vacuum. The crude products were purified on silica gel using a mixture of CH_2Cl_2 /MeOH as eluting system, yielding intermediates **18-22** and **25-28**. The same procedure was repeated to obtain intermediates **23-24** and **29-30** by alkylation of



Scheme 1. A: synthesis of 4-piperazine-indole cores **5** and **6**. Reagents and conditions: i) Boc-piperazine, Pd₂(dba)₃, BINAP, *t*-BuONa, toluene, 110 °C, 5 h; ii) EtOH, 150 °C, MW, 2 h; iii) 3-chlorobenzyl bromide or benzylsulfonyl chloride, BTTP, CH₂Cl₂, 0 °C → rt, 2 h; iv) TFA/CH₂Cl₂, 2/8 v/v, rt, 1 h; **B:** synthesis of alkylating agents **9–17**; i) α,ω-dibromoalkane, K₂CO₃, KOH, KI, acetone, 60 °C, 16 h.



Scheme 2. Synthesis of final compounds **31–48**. Reagents and conditions: i) alkylating agent **9–13** or **14–17**, K₂CO₃, KI, acetone, 60 °C, 16 h; ii) for primary amine: AcOH, THF_{anh}, rt, 5 h then STAB, rt, 2 h; for secondary amine, AcOH, CH₂Cl₂_{anh}, 0.5 h then STAB, rt, 2 h.

1-((3-chlorophenyl)sulfonyl)-4-(piperazin-1-yl)-1*H*-indole with synthesized alkylating agents **11–12** and **15–16**, respectively.

5.1.7. General procedure for reductive amination of ketone with propargyl amine (**31–37**)

Ketone derivative **18** (120 mg, 0.2 mmol, 1 eq), and propargyl amine (26 μL, 0.4 mmol, 2 eq) were solubilized in anhydrous THF (3 mL) and the mixture was stirred for 5 h. The reducing agent STAB (127 mg, 0.6 mmol, 3 eq) was added and the mixture was left stirring for additional 2 h. Subsequently, the reaction was quenched with a saturated solution of NaHCO₃, washed with H₂O (2 ×), brine (1 ×), dried over Na₂SO₄, filtered and concentrated. The obtained crude product was purified using silica gel with CH₂Cl₂/MeOH as an eluting system to obtain final compound **31**. The same procedure was applied to intermediates **19–24** and for yielding final compounds **32–37**.

5.1.8. General procedure for reductive amination of benzaldehyde with *L*-alanamide (**38–43**)

Benzaldehyde derivative **25** (120 mg, 0.25 mmol, 1 eq), and *L*-alanamide hydrochloride (76 mg, 0.5 mmol, 2 eq) were solubilized in anhydrous THF (3 mL) and the mixture was stirred for 5 h. The

the reducing agent STAB (158 mg, 0.75 mmol, 3 eq) was added and the mixture was left stirring for additional 2 h. Subsequently, the reaction was quenched with a saturated solution of NaHCO₃, washed with H₂O (2 ×), brine (1 ×), dried over Na₂SO₄, filtered and concentrated. The obtained crude product was purified using silica gel with CH₂Cl₂/MeOH as an eluting system to obtain final compound **38**. The same procedure was applied to intermediates **26–30** for yielding final compounds **39–43**.

5.1.9. General procedure for reductive amination of benzaldehyde with *N*-methyl-propargyl amine (**44–48**)

Benzaldehyde derivative **26** (120 mg, 0.24 mmol, 1 eq), and *N*-methylpropargyl amine (40 μL, 0.48 mmol, 2 eq) were solubilized in CH₂Cl₂ (3 mL) and the mixture was stirred for 30 min. The reducing agent STAB (152 mg, 0.72 mmol, 3 eq) was added and the mixture was left stirring for additional 1 h. Subsequently, the reaction was quenched with a saturated solution of NaHCO₃, washed with H₂O (2 ×), brine (1 ×), dried over Na₂SO₄, filtered and concentrated. The obtained crude product was purified using silica gel with CH₂Cl₂/MeOH as an eluting system to yield final compound **44**. The same procedure was applied to intermediates **26–30** for yielding final compounds **45–48**.

5.1.10. Characterization data for selected final compounds

5.1.10.1. 4-(4-(4-(1-(3-Chlorobenzyl)-1H-indol-4-yl)piperazin-1-yl)butoxy)-N-(prop-2-yn-1-yl)-2,3-dihydro-1H-inden-1-amine (**33**).

Brown oil, 76 mg (isolated yield 59%) following chromatographic purification over silica gel with CH₂Cl₂/MeOH (9/1, v/v); UPLC/MS purity 98%, *t*_R = 5.14, C₃₅H₃₉ClN₄O, MW 567.17, Monoisotopic Mass 566.28, [M+H]⁺ 567.4. ¹H NMR (500 MHz, CDCl₃) δ ppm 1.27 (m, 2H, N-CH₂-CH₂), 1.38–1.44 (m, 1H, indane), 1.72–1.80 (m, 2H, O-CH₂-CH₂), 1.81–1.91 (m, 3H, indane), 2.25 (t, *J* = 2.4 Hz, 1H, CH≡C-CH₂), 2.55 (t, *J* = 7.3 Hz, 2H, N-CH₂-CH₂), 2.70–2.82 (m, 4H, piperazine), 3.29–3.34 (m, 4H, piperazine), 3.51 (dd, *J* = 5.3, 2.4 Hz, 2H, NH-CH₂-C≡CH), 4.02 (t, *J* = 6.2 Hz, 2H, O-CH₂-CH₂), 4.42 (dd, *J* = 6.9, 5.2 Hz, 1H, CH-NH-CH₂), 5.26 (s, 2H, N-CH₂-Ar), 6.56 (dd, *J* = 2.6, 0.9 Hz, 1H, Ar-H), 6.61 (d, *J* = 7.4 Hz, 1H, Ar-H), 6.73 (d, *J* = 8.3 Hz, 1H, Ar-H), 6.88–6.97 (m, 3H, Ar-H), 7.04–7.12 (m, 3H, Ar-H), 7.14–7.23 (m, 3H, Ar-H). ¹³C NMR (126 MHz, CDCl₃) δ ppm 23.6 (N-CH₂-CH₂), 27.3 (CH₂-indane), 27.5 (O-CH₂-CH₂), 33.1 (CH₂-indane), 36.2 (NH-CH₂-C), 49.7 (N-CH₂-Ar), 51.3 (piperazine), 53.6 (piperazine), 58.5 (N-CH₂-CH₂), 62.4 (CH-indane), 67.7 (O-CH₂-CH₂), 71.5 (CH₂-C≡CH), 82.6 (CH₂-C≡CH), 100.8, 104.4, 106.9, 110.2, 116.5, 122.0, 122.8, 124.9, 126.7, 126.8, 127.9, 130.1, 131.8, 134.8, 137.5, 139.8, 145.9, 146.5, 155.7.

5.1.10.2. (S)-2-((4-(4-(1-(3-Chlorobenzyl)-1H-indol-4-yl)piperazin-1-yl)hexyloxy)benzyl)amino)propanamide (**41**).

Pale yellow oil, 87 mg (isolated yield 64%) following chromatographic purification over silica gel with CH₂Cl₂/MeOH (9/1, v/v); UPLC/MS purity 97%, *t*_R = 4.61, C₃₅H₄₄ClN₅O₂, MW 602.22, Monoisotopic Mass 601.32, [M+H]⁺ 602.3. ¹H NMR (500 MHz, DMSO-*d*₆) δ ppm 1.08 (d, *J* = 6.9 Hz, 3H, NH-CH-CH₃), 1.28–1.36 (m, 2H, N-CH₂-CH₂-CH₂), 1.36–1.42 (m, 2H, O-CH₂-CH₂-CH₂), 1.42–1.49 (m, 2H, N-CH₂-CH₂), 1.63–1.71 (m, 2H, O-CH₂-CH₂), 2.32 (t, *J* = 7.2 Hz, 2H, N-CH₂-CH₂), 2.54 (br. s., 4H, piperazine), 2.96 (q, *J* = 6.9 Hz, 1H, NH-CH-CH₃), 3.07 (br. s., 4H, piperazine), 3.43 (d, *J* = 13.2 Hz, 1H, Ar-CH_{1a}-NH), 3.56 (d, *J* = 13.2 Hz, 1H, Ar-CH_{1b}-NH), 3.89 (t, *J* = 6.6 Hz, 2H, O-CH₂-CH₂), 5.35 (s, 2H, N-CH₂-Ar), 6.40 (d, *J* = 3.4 Hz, 1H, Ar-H), 6.43 (d, *J* = 7.5 Hz, 1H, Ar-H), 6.80–6.84 (m, 2H, CO-NH₂), 6.91–6.97 (m, 2H, Ar-H), 6.99–7.03 (m, 1H, Ar-H), 7.07 (d, *J* = 6.9 Hz, 1H, Ar-H), 7.15–7.21 (m, 3H, Ar-H), 7.24–7.31 (m, 3H, Ar-H), 7.39 (d, *J* = 2.9 Hz, 1H, Ar-H). ¹³C NMR (126 MHz, DMSO-*d*₆) δ ppm 19.8 (CH₃-CH-NH), 26.1 (N-CH₂-CH₂-CH₂), 26.8 (O-CH₂-CH₂-CH₂), 27.3 (N-CH₂-CH₂), 29.3 (O-CH₂-CH₂), 49.0 (N-CH₂-Ar), 51.0 (N-CH₂-CH₂), 51.4 (piperazine), 53.7 (piperazine), 56.9 (NH-CH-CH₃), 58.5 (O-CH₂-CH₂), 67.9 (Ar-CH₂-NH), 100.7, 104.9, 106.6, 114.6, 121.8, 122.6, 126.2, 127.2, 127.8, 129.7, 131.0, 132.7, 133.7, 137.3, 141.5, 146.1, 158.1, 177.4 (C=O).

5.1.10.3. (S)-2-((4-(4-(1-(Phenylsulfonyl)-1H-indol-4-yl)piperazin-1-yl)butoxy)benzyl)amino)propanamide (**42**).

Pale yellow oil, 82 mg (isolated yield 60%) following chromatographic purification over silica gel with CH₂Cl₂/MeOH (9/1, v/v); UPLC/MS purity 96%, *t*_R = 4.41, C₃₂H₃₉N₅O₄S, MW 589.76, Monoisotopic Mass 589.27, [M+H]⁺ 590.4. ¹H NMR (500 MHz, CDCl₃) δ ppm 1.35 (d, *J* = 6.9 Hz, 3H, NH-CH-CH₃), 1.67–1.76 (m, 2H, N-CH₂-CH₂), 1.78–1.86 (m, 2H, O-CH₂-CH₂), 2.51 (t, *J* = 6.3 Hz, 2H, N-CH₂-CH₂), 2.68 (br. s., 4H, piperazine), 3.15 (br. s., 4H, piperazine), 3.22 (q, *J* = 6.3 Hz, 1H, NH-CH-CH₃), 3.63–3.74 (m, 2H, Ar-CH₂-NH), 3.97 (t, *J* = 6.0 Hz, 2H, O-CH₂-CH₂), 5.59 (br. s., 1H, CO-NH_{1a}), 6.66 (d, *J* = 4.0 Hz, 1H, Ar-H), 6.71 (d, *J* = 7.4 Hz, 1H, Ar-H), 6.82–6.87 (m, 2H, Ar-H), 7.09 (br. s., 1H, CO-NH_{1b}), 7.15–7.23 (m, 3H, Ar-H), 7.38–7.43 (m, 2H, Ar-H), 7.46–7.55 (m, 2H, Ar-H), 7.63 (d, *J* = 8.0 Hz, 1H, Ar-H), 7.85 (d, *J* = 7.4 Hz, 2H, Ar-H). ¹³C NMR (126 MHz, CDCl₃) δ ppm 19.8 (CH₃-CH-NH), 23.4 (N-CH₂-CH₂), 27.3 (O-CH₂-CH₂), 29.8 (piperazine), 51.5 (piperazine), 52.1 (N-CH₂-CH₂), 53.5 (piperazine), 57.7 (NH-CH-CH₃), 58.3 (O-CH₂-CH₂), 67.8 (Ar-CH₂-NH), 107.5,

108.0, 110.9, 114.6, 124.2, 124.9, 125.6, 126.9, 129.3, 131.6, 133.9, 136.0, 138.3, 146.1, 158.4, 178.2 (C=O).

5.1.10.4. N-(4-((5-(4-(1-(3-Chlorobenzyl)-1H-indol-4-yl)piperazin-1-yl)pentyl)oxy)benzyl)-N-methylprop-2-yn-1-amine (**45**).

Pale yellow oil, 99 mg (isolated yield 75%) following chromatographic purification over silica gel with CH₂Cl₂/MeOH (9/0.7, v/v); UPLC/MS purity 100%, *t*_R = 5.73, C₃₅H₄₁ClN₄O, MW 569.19, Monoisotopic Mass 568.30, [M+H]⁺ 569.4. ¹H NMR (500 MHz, CDCl₃) δ ppm 1.47–1.56 (m, 2H, O-CH₂-CH₂-CH₂), 1.61–1.70 (m, 2H, N-CH₂-CH₂), 1.79–1.86 (m, 2H, O-CH₂-CH₂), 2.23–2.28 (m, 1H, CH≡C-CH₂), 2.33 (s, 3H, N-CH₃), 2.46–2.54 (m, 2H, N-CH₂-CH₂), 2.74 (br. s., 4H, piperazine), 3.28 (d, *J* = 2.3 Hz, 2H, N-CH₂-C≡CH), 3.32 (br. s., 4H, piperazine), 3.50 (s, 2H, CH₃-N-CH₂-Ar), 3.96 (t, *J* = 6.4 Hz, 2H, O-CH₂-CH₂), 5.25 (s, 2H, N-CH₂-Ar), 6.56 (d, *J* = 3.2 Hz, 1H, Ar-H), 6.59–6.62 (m, 1H, Ar-H), 6.85 (d, *J* = 8.6 Hz, 2H, Ar-H), 6.91 (dd, *J* = 10.9, 7.2 Hz, 2H, Ar-H), 7.04–7.11 (m, 3H, Ar-H), 7.16–7.27 (m, 4H, Ar-H). ¹³C NMR (126 MHz, CDCl₃) δ ppm 24.2 (N-CH₂-CH₂-CH₂), 26.7 (N-CH₂-CH₂), 29.3 (piperazine), 29.8 (piperazine), 30.4 (O-CH₂-CH₂), 41.8 (N-CH₃), 44.7 (N-CH₂-CH₂), 49.7 (N-CH₂-Ar), 51.3 (piperazine), 53.7 (piperazine), 58.8 (O-CH₂-CH₂), 59.4 (Ar-CH₂-N-CH₃), 67.9 (CH₂-C≡CH), 73.4 (CH₂-C≡CH), 78.7 (CH₂-C≡CH), 100.8, 104.4, 106.9, 114.4, 122.1, 122.8, 124.9, 126.7, 126.8, 127.9, 130.1, 130.3, 130.5, 134.8, 137.5, 139.8, 145.9, 158.4.

5.1.10.5. N-methyl-N-(4-(4-(4-(1-(phenylsulfonyl)-1H-indol-4-yl)piperazin-1-yl)butoxy)benzyl)prop-2-yn-1-amine (**47**).

Pale yellow oil, 100 mg (isolated yield 75%) following chromatographic purification over silica gel with CH₂Cl₂/MeOH (9/0.7, v/v); UPLC/MS purity 97%, *t*_R = 4.49, C₃₃H₃₈N₄O₃S, MW 570.75, Monoisotopic Mass 570.27, [M+H]⁺ 571.4. ¹H NMR (500 MHz, CDCl₃) δ ppm 1.67–1.75 (m, 2H, N-CH₂-CH₂), 1.79–1.85 (m, 2H, O-CH₂-CH₂), 2.25 (t, *J* = 2.3 Hz, 1H, CH≡C-CH₂), 2.31 (s, 3H, N-CH₃), 2.49 (t, *J* = 7.4 Hz, 2H, N-CH₂-CH₂), 2.58–2.74 (m, 4H, piperazine), 3.15 (t, *J* = 4.3 Hz, 4H, piperazine), 3.27 (d, *J* = 2.3 Hz, 2H, N-CH₂-C≡CH), 3.49 (s, 2H, CH₃-N-CH₂-Ar), 3.97 (t, *J* = 6.3 Hz, 2H, O-CH₂-CH₂), 6.67 (dd, *J* = 3.7, 0.9 Hz, 1H, Ar-H), 6.71 (d, *J* = 7.7 Hz, 1H, Ar-H), 6.82–6.86 (m, 2H, Ar-H), 7.18–7.26 (m, 3H, Ar-H), 7.37–7.45 (m, 2H, Ar-H), 7.48–7.53 (m, 2H, Ar-H), 7.64 (d, *J* = 8.3 Hz, 1H, Ar-H), 7.83–7.88 (m, 2H, Ar-H). ¹³C NMR (126 MHz, CDCl₃) δ ppm 23.5 (N-CH₂-CH₂), 27.4 (O-CH₂-CH₂), 41.8 (N-CH₃), 44.7 (N-CH₂-CH₂), 51.6 (piperazine), 53.5 (piperazine), 58.4 (O-CH₂-CH₂), 59.4 (Ar-CH₂-N-CH₃), 67.7 (CH₂-C≡CH), 73.4 (CH₂-C≡CH), 78.7 (CH₂-C≡CH), 107.6, 107.9, 110.9, 114.4, 124.3, 124.8, 125.6, 126.9, 129.3, 130.4, 133.9, 136.0, 138.3, 146.2, 158.4.

5.1.10.6. N-methyl-N-(4-((5-(4-(1-(phenylsulfonyl)-1H-indol-4-yl)piperazin-1-yl)pentyl)oxy)benzyl)prop-2-yn-1-amine (**48**).

Pale yellow oil, 103 mg (isolated yield 78%) following chromatographic purification over silica gel with CH₂Cl₂/MeOH (9/0.7, v/v); UPLC/MS purity 100%, *t*_R = 4.61, C₃₃H₃₈N₄O₃S, MW 584.78, Monoisotopic Mass 584.28, [M+H]⁺ 585.5. ¹H NMR (500 MHz, CDCl₃) δ ppm 1.48–1.56 (m, 2H, O-CH₂-CH₂-CH₂), 1.60–1.67 (m, 2H, N-CH₂-CH₂), 1.79–1.86 (m, 2H, O-CH₂-CH₂), 2.28 (t, *J* = 2.6 Hz, 1H, CH≡C-CH₂), 2.33 (s, 3H, N-CH₃), 2.47 (t, *J* = 7.4 Hz, 2H, N-CH₂-CH₂), 2.68 (br. s., 4H, piperazine), 3.18 (t, *J* = 4.6 Hz, 4H, piperazine), 3.29 (d, *J* = 2.3 Hz, 2H, N-CH₂-C≡CH), 3.51 (s, 2H, CH₃-N-CH₂-Ar), 3.96 (t, *J* = 6.3 Hz, 2H, O-CH₂-CH₂), 6.68–6.70 (m, 1H, Ar-H), 6.73 (d, *J* = 7.5 Hz, 1H, Ar-H), 6.83–6.87 (m, 2H, Ar-H), 7.20–7.26 (m, 3H, Ar-H), 7.40–7.44 (m, 2H, Ar-H), 7.50–7.53 (m, 1H, Ar-H), 7.53 (d, *J* = 3.4 Hz, 1H, Ar-H), 7.66 (d, *J* = 8.6 Hz, 1H, Ar-H), 7.86–7.87 (m, 1H, Ar-H), 7.88–7.89 (m, 1H, Ar-H). ¹³C NMR (126 MHz, CDCl₃) δ ppm 24.2 (N-CH₂-CH₂-CH₂), 26.6 (N-CH₂-CH₂), 29.3 (O-CH₂-CH₂), 41.7 (N-CH₃), 44.7

(N-CH₂-CH₂), 51.5 (piperazine), 53.5 (piperazine), 58.7 (O-CH₂-CH₂), 59.4 (Ar-CH₂-N-CH₃), 67.8 (CH₂-C≡CH), 73.4 (CH₂-C≡CH), 78.7 (CH₂-C≡CH), 107.6, 108.0, 110.9, 114.4, 124.3, 124.9, 125.6, 126.9, 129.3, 130.3, 130.5, 133.9, 136.0, 138.3, 146.2, 158.4. Anal. calcd for dihydrochloride dihydrate salt C₃₃H₃₈N₄O₃S·2HCl·2H₂O: C: 58.87, H: 6.68, N: 8.08, S: 4.62; Found C: 59.03, H: 6.44, N: 7.72, S: 4.39. M.p. for C₃₃H₃₈N₄O₃S·2HCl·2H₂O: 215.1–219.3 °C.

5.2. In silico simulations

5.2.1. Molecular docking

The 5-HT₆R homology models were obtained according to the procedure described before on the β₂ receptor template and successfully used in our earlier studies of different groups of 5-HT₆R ligands simulations [51,52]. The structure of monoamine oxidases B (PDB code 2C65)⁴¹ in complex with irreversible inhibitor rasagiline analog (4-(N-methyl-N-ethyl-carbamoyloxy)-N-methyl-N-propargyl-1(R)-aminoindan) was fetched from the Protein Data Bank. The structures of the 5-HT₆ receptor and MAO-B enzyme were optimized using the induced-fit docking (IFD) procedure from Schrödinger Suite. The IFD combines flexible ligand docking with target structure prediction and side chain refinement. The structure of **48** was used as input to IFD. Centroid of the grid box was anchored on D3.32 and I199 in 5-HT₆ and MAO-B, respectively. Due to the size of the input ligand, it allowed on residue refinement within 12 Å and 33 Å of ligand poses for 5-HT₆ and MAO-B, respectively. The Extended Sampling Protocol was used, which generates up to 80 poses per ligand by automated docking. All obtained L–R complexes were inspected visually to select those that displayed the closest compliance with the common binding mode for studied protein targets. Final validation of the selected conformations was performed by docking (Glide SP mode) the designed library, retaining only those with a coherent binding mode [53]. The 3-dimensional structures of the ligands were obtained using LigPrep v3.6,⁵⁴ and the appropriate ionization states at pH = 7.4 ± 1.0 were assigned using Epik v3.4 [55].

5.2.2. QM/MM optimization

The L–R complexes selected in IFD procedure were next optimized using QM/MM approach using QSite. The QM region contained ligand and amino acid side chain directly interacting with the ligand was described by a combination of DFT hybrid functional B3LYP and LACVP* basis set, while the rest of the system was optimized using OPLS2005 force field.

5.2.3. Covalent docking

The CovDock workflow [56] from Schrödinger Suite was used for pose prediction and scoring of covalently bound ligands to a flavin adenine dinucleotide cofactor (FAD) presence in catalytic site of MAO-B enzyme. The reaction between FAD and propargyl group was not pre-defined in CovDock library, thus we used custom reaction editor to describe the reaction based on the mechanism proposed by Tandarić et al. [42] At first, we defined in SMARTS language the fragments of the ligand [C#CC[N,n]] and FAD [[nH]c(=O)cNc] between which the reaction occurs. The grid center was set to I199, assuming its size to 33 Å. The rest setting was used as default.

5.3. In vitro pharmacological evaluation

5.3.1. Radioligand binding assays

All experiments were carried out according to the previously published procedures [57–59]. HEK293 cells stably expressing human 5-HT_{1A}, 5-HT₆, 5-HT_{7b} and D_{2L} receptors (prepared with the

use of Lipofectamine 2000) or CHO–K1 cells with plasmid containing the sequence coding for the human serotonin 5-HT_{2A} receptor (PerkinElmer) were maintained at 37 °C in a humidified atmosphere containing 5% CO₂ and grown in Dulbecco's Modified Eagle's Medium containing 10% dialyzed fetal bovine serum and 500 µg/mL G418 sulfate. For membrane preparation, cells were cultured in 150 cm² flasks, grown to 90% confluence, washed twice with pre-warmed to 37 °C phosphate buffered saline (PBS) and centrifuged (200×g) in PBS containing 0.1 mM EDTA and 1 mM dithiothreitol. Prior to membrane preparation, pellets were stored at –80 °C.

Cell pellets were thawed and homogenized in 10 vol of assay buffer using an Ultra Turrax tissue homogenizer and centrifuged twice at 35 000×g for 15 min at 4 °C, with incubation for 15 min at 37 °C between the centrifugations. The composition of the assay buffers was experimentally selected to achieve the maximum signal window (more details in SI). All assays were carried out in a total volume of 200 µL in 96-well plates for 1 h at 37 °C, except 5-HT_{1A}R and 5-HT_{2A}R which were incubated at room temperature and 27 °C, respectively. The process of equilibration was terminated by rapid filtration through Unifilter plates with a 96-well cell harvester and radioactivity retained on the filters was quantified on a Microbeta plate reader (PerkinElmer, USA). For displacement studies the assay samples contained as radioligands (PerkinElmer, USA): 2.5 nM [³H]-8-OH-DPAT (135.2 Ci/mmol) for 5-HT_{1A}R; 1 nM [³H]-ketanserin (53.4 Ci/mmol) for 5-HT_{2A}R; 2 nM [³H]-LSD (83.6 Ci/mmol) for 5-HT₆R; 0.8 nM [³H]-5-CT (39.2 Ci/mmol) for 5-HT₇R or 2.5 nM [³H]-raclopride (76.0 Ci/mmol) for D_{2L}R. Non-specific binding was defined in the presence of 10 µM of 5-HT in 5-HT_{1A}R and 5-HT₇R binding experiments, whereas 20 µM of mianserin, 10 µM of methiothepine or 10 µM of haloperidol were used in 5-HT_{2A}R, 5-HT₆R and D_{2L} assays, respectively. Each compound was tested in triplicate at 7 concentrations (10^{–10}–10^{–4} M). The inhibition constants (K_i) were calculated from the Cheng-Prusoff equation [60].

Additionally, the affinity of compound **48** for α₁ and β₁-adren-ergic receptors, histaminic H₁ and muscarinic M₁ receptors were evaluated at Eurofins. The results were expressed as the % inhibition of the control binding according to experimental protocols described online at <https://www.eurofins.com/>.

5.3.2. Monoamine oxidase assays

Inhibition activity of evaluated compounds was measured using human recombinant MAO-B and MAO-A (Sigma Aldrich M7441 and M7316) in the fluorometric method for detecting monoamine oxidase activity. The assay was carried out in 96-well plate. 2 µL of appropriate concentration of tested compounds in DMSO were added to wells that contained 98 µL of enzyme dilution (0.53 U/ml) in phosphate buffer (50 mM, pH 7.4). After the 30 min of pre-incubation in room temperature 50 µL of the solution of 800 µM 10-Acetyl-3,7-dihydroxyphenoxazine (Cayman Chemical Company 10010469) and 4 U/mL horse radish peroxidase (HRP, Sigma Aldrich P6782) was added and enzymatic reaction was started by addition of 50 µL of 800 µM p-tyramine (Alfa Aesar A12220) solution. The signal was measured after 1 h (excitation at 570 nm and emission at 585 nm) using EnSpire® multimode plate reader (PerkinElmer, Inc.). Rasagiline (1 µM) or clorgyline (1 µM) were tested as reference compounds for MAO-B and MAO-A inhibitions, respectively [61,62].

5.3.3. Reversibility studies

To investigate reversibility of MAO-B inhibition compound **48**, rasagiline and safinamide were tested in concentration corresponding to their IC₈₀ values. Experiment was carried out in 96-well plate divided into two parts. In the first portion hMAO-B was

incubated with inhibitors for 30 min. In the second portion of inhibitors were added to hMAO-B directly before the next step. Then 10 μ M p-tyramine and the solution of 800 μ M 10-acetyl-3,7-dihydroxyphenoxazine and 4 U/mL HRP were added to both parts of the plate. Fluorescence signal had been measured in the microplate reader for 22 min then the concentration of p-tyramine was increased to 1 mM. After addition of p-tyramine fluorescence was measured every 5 min for 5 h [62].

5.3.4. Determination of cAMP production in 1321N1 cells

The properties of compound **48** to inhibit cAMP production induced by 5-CT (1000 nM), a 5-HT₆R agonist, was evaluated. Compounds were tested in triplicate at 8 concentrations (10^{-11} – 10^{-4} M). The level of cAMP was measured using frozen recombinant 1321N1 cells expressing the Human Serotonin 5-HT₆R (PerkinElmer). Total cAMP was measured using the LANCE cAMP detection kit (PerkinElmer), according to the manufacturer's recommendations. For quantification of cAMP levels, 2000 cells/well (5 μ L) were incubated with mixture of compounds (5 μ L) for 30 min at room temperature in 384-well white opaque microtiter plate. After incubation, the reaction was stopped and cells were lysed by the addition of 10 μ L of working solution (5 μ L Eu-cAMP and 5 μ L ULight-anti-cAMP) for 1 h at room temperature. Time-resolved fluorescence resonance energy transfer (TR-FRET) was detected by an Infinite M1000 Pro (Tecan) using instrument settings from LANCE cAMP detection kit manual. K_b values were calculated from Cheng–Prusoff equation specific for the analysis of functional inhibition curves: $K_b = IC_{50}/(1+A/EC_{50})$ where A represents agonist concentration, IC_{50} the concentration of antagonist producing a 50% reduction in the response to agonist, and EC_{50} the agonist concentration which causes a half of the maximal response [60].

5.3.5. Determination of cAMP production in NG108-15 cells

NG108-15 cells were grown in Dulbecco's modified Eagle's medium (DMEM) supplemented with 10% dialyzed fetal calf serum, 2% hypoxanthine/aminopterin/thymidine (Life technologies), and antibiotics. cAMP measurement was performed in cells transiently expressing 5-HT₆R using the bioluminescence resonance energy transfer (BRET) sensor for cAMP, CAMYEL (cAMP sensor using YFP-Epac-RLuc) [63]. NG108-15 cells were co-transfected in suspension with 5-HT₆R (0.5 μ g DNA/million cells) and CAMYEL constructs (1 μ g DNA/million cells), using Lipofectamine 2000, according to the manufacturer's protocol, and plated in white 96-well plates (Greiner), at a density of 50 000 cells per well. Twenty-four h after transfection, cells were washed with PBS containing calcium and magnesium. To test the inverse agonist properties of compound **48** and intepirdine, cells were treated with vehicle or with the tested compound at incremental concentrations of these compounds (from 0.1 nM to 10 μ M). Coelenterazine H (Molecular Probes) was added at a final concentration of 5 μ M, and left at room temperature for 5 min. BRET was measured using a Mithras LB 940 plate reader (Berthold Technologies). Expression of 5-HT₆R in NG108-15 cells induced a strong decrease in CAMYEL BRET signal, compared with cells transfected with an empty vector instead of the plasmid encoding the 5-HT₆R. This decrease in CAMYEL BRET signal was thus used as an index of 5-HT₆R constitutive activity at Gs signaling.

5.4. Assessment of preliminary ADME/Tox properties

5.4.1. PAMPA – parallel artificial membrane permeability assay

Parallel artificial membrane permeability assay (PAMPA) was performed using Corning® Gentest™ Pre-coated PAMPA Plate System, according to the manufacturer's instructions. Compound

48 (100 μ M) was incubated on plates in phosphate-buffer saline (pH 7.4) for 5 h at room temperature. Concentrations of **48** in donor and acceptor solutions were determined using UPLC-MS with the internal standard based on pentoxifylline method. Membrane permeability expressed as logPe was calculated as follows:

$$\log Pe = \log \left(\frac{-\ln \left[1 - \frac{C_A}{C_D \times \frac{V_D + C_A \times V_A}{V_D + V_A}} \right]}{A \times \left(\frac{1}{V_D} + \frac{1}{V_A} \right) \times t} \right)$$

where CD and CA are the final concentrations after incubation and VD, VA - volumes of the donor and the acceptor solutions (0.3 mL, 0.2 mL), respectively. A - membrane surface area (0.3 cm²), t - incubation time (18 000 s). Two reference standards were used in the study – verapamil (Pe = 1.85×10^{-5} cm/s) – a well permeable drug and doxorubicin (Pe = ND, not detected in acceptor compartment) – no membrane penetration properties.

5.4.2. In vitro metabolic stability studies

Metabolic stability of tested compound was analyzed using incubation systems, composed of: tested compound (10 μ M), rat liver microsomes (RLMs, microsomes from rat male liver, pooled; 0.4 mg/mL; Sigma Aldrich), NADPH-regenerating system (NADP⁺, glucose-6-phosphate and glucose-6-phosphate dehydrogenase in 100 mM potassium buffer, pH 7.4; all from Sigma Aldrich) and potassium buffer, pH 7.4. Stock solution of tested compounds was prepared in methanol (the final methanol concentration in incubation mixture does not exceed 0.1%). Firstly, all samples contained incubation mixture (without NADPH-regenerating system) were pre-incubated in thermoblock at 37 °C, for 10 min. Then reaction was initiated by the addition of NADPH-regenerating system. In control samples NADPH-regenerating system was replaced with potassium buffer. Probes were incubated for 30 and 60 min at 37 °C. After addition of internal standard (pentoxifylline, 10 μ M) biotransformation process was stopped by addition of perchloric acid. Next, samples were centrifuge and supernatants were analyzed using UPLC/MS (Waters Corporation, Milford, MA). All experiments were run in duplicates. Half-life time was evaluated using non-linear regression model using Graph Pad Prism software and intrinsic clearance was calculated from the equation $Cl_{int} = (\text{volume of incubation } [\mu\text{L}]/\text{protein in the incubation } [\text{mg}]) \times 0.693/t_{1/2}$ [64].

5.4.3. Evaluation of hepatotoxicity

5.4.3.1. Cell culture. Human liver cancer cells HepG2 (ATCC 59195) were cultured in EMEM media supplemented with 10% FBS at 37 °C, in a humidified atmosphere with 5% CO₂ and antibiotics. Cells were incubated in the presence of compounds for 24 h. The anti-proliferative drug DOX was used as a positive control in concentration range of 0.1–25 μ M.

5.4.3.2. MTT assay. Cell viability was estimated by using the MTT assay, which assesses the ability mitochondrial dehydrogenases to reduce tetrazolium salts into a colored formazan compound [65]. At the end of the incubation period, 10 μ L of MTT (5 mg/mL) were added to each well. After 4 h, formazan crystals were solubilized with DMSO and optical density was measured at 570 nm by using a SpectraMax iD3 Multi-Mode Microplate Reader (Molecular Devices). Each experiment was performed in triplicate and repeated three times.

5.4.4. Preliminary in vivo pharmacokinetics experiments

5.4.4.1. Instrumentation and operating conditions. The LC/ESI-MS/MS experiments were performed on an ABSciex (Concord,

Ontario, Canada) API 3200 triple quadrupole mass spectrometer equipped with an electrospray (ESI) ionization interface. This instrument was coupled to Shimadzu (Shimadzu, Japan) LC system. Data acquisition and processing were accomplished using ABSciex Analyst 1.5.2 data collection and integration software.

5.4.4.2. Chromatographic and mass spectrometric conditions. Acclaim Polar Advantage II (3.0 mm × 74 mm, 3 μm, 120A, Dionex, USA) analytical column was used for compound separation. The temperatures of the column thermostat and the autosampler were set at 40 °C and 10 °C, respectively. The mobile phase consisted of a mixture of acetonitrile with addition of 0.1% formic acid (solvent A) and water with addition of 0.1% formic acid (solvent B) and was set at a flow rate of 0.4 mL min⁻¹. Starting amount of solvent A is 10%, isocratic elution from 0 to 5 min, and then gradient up to 90% of solvent A, and maintained to 10 min, and then gradient down to 10% of solvent A, and maintained to 15 min. To find the optimal parameters of ion path and ion source for studied compound the quantitative optimization was done by direct infusion of the molecule at a concentration of 1 μg/mL, and at a flow rate of 10 μL/min using a Hamilton syringe pump (Hamilton, Reno, Nevada). The ion source parameters were as follows: ion spray voltage: 4500 V; nebulizer gas (gas 1): 20 psi; turbo gas (gas 2): 20 psi; temperature of the heated nebulizer: 400 °C; curtain gas: 40 psi; collision gas: 6 psi. Mass spectra were acquired by SRM with precursor/predominant product ion transitions for the analyte. The mass spectral Q1 → Q3 transitions monitored for compound **48** and for IS were *m/z* 585.1 → 516.2 and *m/z* 305 → 248, respectively. The peak widths of precursor and product ions were set to 0.7 full width half-height. Quantification was done via peak area ratio.

5.4.4.3. Sample pretreatment. The plasma and brain sample pretreatment procedure involved acetonitrile precipitation. A 5 μL aliquot of the internal standard (IS, PH003437, Merck, Darmstadt, Germany). working solution (5 μg/mL) was added to 100 μL of the collected rat plasma sample, which was then vortex-mixed for 10 s. Thereafter, 200 μL of acetonitrile was added, vortexed during 20 min, and then centrifuged (10 000 rpm, 10 min). The supernatant (200 μL) was then transferred to insert placed in an autosampler vial, and a 20 μL volume of this was injected onto the LC column. Brain samples were thawed before use, and whole brain were weighted and placed in a glass mortar and pestle tissue grinder, and homogenized with an appropriate amount of phosphate buffer (pH 7.4) in 1:2.5 ratio. Afterward, 100 μL of tissue homogenates were transferred to new Eppendorf tubes and spiked with 5 μL of the internal standard working solution. All samples were stored on ice during the preparation process and followed by procedures similar to those described above.

5.4.4.4. Animals. A group of 32 adult male rats (Wistar, 200–220 g) were used in the experiment. The animals were purchased from the Animal House at the Faculty of Pharmacy, Jagiellonian University Medical College, Krakow, Poland. During the habituation period the groups of 4 rats were kept in a plastic cage at a controlled room temperature (22 ± 2 °C), humidity (55 ± 10%), full spectrum cold white light (350–400 lx), on 12 h light/12 dark cycles (the lights on at 7:00 a.m., and off at 19:00 p.m.), and had free access to standard laboratory pellet and tap water. For pharmacokinetic study compound **48** dissolved in saline were administered by intragastric gavage at a dose of 3 mg/kg. Blood samples were collected at 0 min (predose), 5 min, 15 min, 30 min, 60 min, 120 min, 240 min and 480 min after compound administration. The blood and brain samples were collected under general anesthesia induced by *i.p.* injection of 50 mg/kg ketamine plus 8 mg/kg xylazine. The blood samples were taken into heparinized tubes, immediately

centrifuged at 1000×g for 10 min, and plasma was collected. The plasma and brain samples were immediately frozen at –80 °C. All experimental procedures were carried out in accordance with EU Directive 2010/63/EU and approved by the I Local Ethics Committee for Experiments on Animals of the Jagiellonian University in Krakow, Poland.

5.5. Assessment of glioprotecting properties

5.5.1. Cell culture

Astrocytes (C8-D1A cells) were cultured in 25 cm² flask with DMEM supplemented with 10% FBS at 37 °C, in a humidified atmosphere with 5% CO₂ until the cells reached 80–90% confluence. Cells were harvested and seeded in 96-well plates at a density of 1 × 10⁴ cells per well. They were pre-incubated with tested compounds analyzed compounds for 12 h, then 6-OHDA (25 μM) was added for next 24 h. The ability of compounds to prevent 6-OHDA-induced cytotoxicity was assessed by using the MTT and LDH assays.

5.5.2. MTT assay

Cell viability was estimated by using the MTT assay, which assesses the ability mitochondrial dehydrogenases to reduce tetrazolium salts into a colored formazan compound [65]. At the end of the incubation period, 10 μL of MTT (5 mg/mL) were added to each well. After 4 h, formazan crystals were solubilized with DMSO and optical density was measured at 570 nm by using a SpectraMax iD3 Multi-Mode Microplate Reader (Molecular Devices). Each experiment was performed in triplicate and repeated three times.

5.5.3. LDH assay

Cells were seeded at density 3 × 10⁴ cells/per well in 96 well plates. After 24 h selegiline, intepirdine, and compound **48** were added to final concentrations of 0.25 μM. After 24 h pre-incubation, 6-OHDA (25 μM) was added to the cultures for an additional 24-h period to induce astrocyte injury. Then, plates were centrifuged (200×g, 2 min) and 50 μL of the supernatant were transferred into the corresponding 96-well plate. Subsequently, 50 μL of LDH-reaction mixture prepared according to the manufacturer's instructions (Invitrogen) were added to each well. Incubation was conducted in darkness for 30 min at room temperature. Next, stop solution was added and absorbance was measured at 490 nm (A490) using a plate reader (Spectra Max iD3, Molecular Devices). Cytotoxicity was determined as follows: cytotoxicity (%) = [(compound LDH activity – spontaneous LDH activity)/(maximum LDH activity – spontaneous LDH activity)] × 100. The maximum LDH activity was prepared by treating cells with lysis buffer (control +). The medium used in the LDH assay contained 1% FBS. Three independent experiments were performed for each condition.

5.6. In vivo pharmacological evaluation

The experiments were performed according to the previously reported procedures [66,67] and were conducted in accordance with the NIH Guide for the Care and Use of Laboratory Animals and were approved by the Ethics Committee for Animal Experiments, Institute of Pharmacology. Male Sprague–Dawley rats (Charles River, Germany) weighing ~250 g at the arrival were housed in the standard laboratory cages, under standard colony A/C controlled conditions: room temperature 21 ± 2 °C, humidity (40–50%), 12-hr light/dark cycle (lights on: 06:00) with ad libitum access to food and water. Rats were allowed to acclimatize for at least 7 days before the start of the experimental procedure. During this week animals were handled for at least 3 times. Behavioral testing was

carried out during the light phase of the light/dark cycle. At least 1 h before the start of the experiment, rats were transferred to the experimental room for acclimation. Rats were tested in a dimly lit (25 lx) "open field" apparatus made of a dull gray plastic (66 × 56 × 30 cm). After each measurement, the floor was cleaned and dried.

5.6.1. Drug treatment

Scopolamine hydrobromide used to attenuate learning, was purchased from Sigma Aldrich (Germany). Scopolamine and tested compound **48** were solubilized in distilled water and then administered at the dose of 1.25 mg/kg (*i.p.*) and 1–3 mg/kg (*p.o.*) 30 and 120 min before familiarization phase (T1), respectively.

5.6.2. Experimental procedure

Procedure consisted of habituation to the arena (without any objects) for 5 min, 24 h before the test and test session comprised of two trials separated by an inter trial interval (ITI). For scopolamine (SCOP)-induced memory impairment paradigm, 1 h ITI was chosen. During the first trial (familiarization, T1) two identical objects (A1 and A2) were presented in opposite corners, approximately 10 cm from the walls of the open field. In the second trial (recognition, T2) one of the objects was replaced by a novel one (A = familiar and B = novel). Both trials lasted 3 min and animals were returned to their home cage after T1. The objects used were the glass beakers filled with the gravel and the plastic bottles filled with the sand. The heights of the objects were comparable (~12 cm) and the objects were heavy enough not to be displaced by the animals. The sequence of presentations and the location of the objects was randomly assigned to each rat. The animals explored the objects by looking, licking, sniffing or touching the object while sniffing, but not when leaning against, standing or sitting on the object. Any rat spending less than 5 s exploring the two objects within 3 min of T1 or T2 was eliminated from the study. Exploration time of the objects and the distance travelled were measured using the Any-maze® video tracking system. Based on exploration time (E) of two objects during T2, discrimination index (DI) was calculated according to the formula: $DI = (EB - EA) / (EA + AB)$.

Declaration of competing interest

The authors declare that they have no known competing financial interests or personal relationships that could have appeared to influence the work reported in this paper.

Acknowledgements

The authors acknowledge the financial support from the National Science Centre, Poland (grant no. 2016/21/B/NZ7/01742). SCD and PM were supported by grants from CNRS, INSERM, Montpellier University of Excellence (iSITE MUSE), the French Foundation for Medical Research (FRM) and ANR (ANR-17-CE16-0013-01 and ANR-17-CE16-0010-01).

Appendix A. Supplementary data

Supplementary data to this article can be found online at <https://doi.org/10.1016/j.ejmech.2020.112765>.

References

- [1] S.R.A. Devenish, The current landscape in Alzheimer's disease research and drug discovery, *Drug Discov. Today* 25 (6) (2020) 943–945.
- [2] B. De Strooper, Lessons from a failed γ -secretase Alzheimer trial, *Cell* 159 (4) (2014) 721–726.
- [3] F. Panza, M. Lozupone, V. Solfrizzi, R. Sardone, C. Piccininni, V. Dibello,

- R. Stallone, G. Giannelli, A. Bellomo, A. Greco, et al., BACE Inhibitors in clinical development for the treatment of Alzheimer's disease, *Expert Rev. Neurother.* 18 (11) (2018) 847–857.
- [4] M. Andrews, B. Tousi, M.N. Sabbagh, 5-HT₆ Antagonists in the treatment of Alzheimer's dementia: current progress, *Neurol. Ther.* 7 (1) (2018) 51–58.
- [5] J.-H. Park, Y.H. Ju, J.W. Choi, H.J. Song, B.K. Jang, J. Woo, H. Chun, H.J. Kim, S.J. Shin, O. Yarishkin, et al., Newly developed reversible MAO-B inhibitor circumvents the shortcomings of irreversible inhibitors in Alzheimer's disease, *Sci. Adv.* 5 (3) (2019) eaav0316.
- [6] M.L. Bolognesi, Polypharmacology in a single drug: multitarget drugs, *Curr. Med. Chem.* 20 (13) (2013) 1639–1645.
- [7] M.L. Bolognesi, Harnessing polypharmacology with medicinal chemistry, *ACS Med. Chem. Lett.* 10 (3) (2019) 273–275.
- [8] X.-Y. Jiang, T.-K. Chen, J.-T. Zhou, S.-Y. He, H.-Y. Yang, Y. Chen, W. Qu, F. Feng, H.-P. Sun, Dual GSK-3 β /AChE inhibitors as a new strategy for multitargeting anti-Alzheimer's disease drug discovery, *ACS Med. Chem. Lett.* 9 (3) (2018) 171–176.
- [9] B. Kumar, V. Kumar, V. Prashar, S. Saini, A.R. Dwivedi, B. Bajaj, D. Mehta, J. Parkash, V. Kumar, Dipropargyl substituted diphenylpyrimidines as dual inhibitors of monoamine oxidase and acetylcholinesterase, *Eur. J. Med. Chem.* 177 (2019) 221–234.
- [10] R. Farina, L. Pisani, M. Catto, O. Nicolotti, D. Gadaleta, N. Denora, R. Soto-Otero, E. Mendez-Alvarez, C.S. Passos, G. Muncipinto, et al., Structure-based design and optimization of multitarget-directed 2H-Chromen-2-one derivatives as potent inhibitors of monoamine oxidase B and cholinesterases, *J. Med. Chem.* 58 (14) (2015) 5561–5578.
- [11] F. Prati, A. De Simone, P. Bisignano, A. Armirotti, M. Summa, D. Pizzirani, R. Scarpelli, D.I. Perez, V. Andrisano, A. Perez-Castillo, et al., Multitarget drug discovery for Alzheimer's disease: triazinones as BACE-1 and GSK-3 β inhibitors, *Angew. Chem., Int. Ed. Engl.* 54 (5) (2015) 1578–1582.
- [12] O.M. Saavedra, D. Karila, D. Brossard, A. Rojas, D. Dupuis, A. Gohier, C. Mannoury la Cour, M.J. Millan, J.C. Ortuno, S. Hanessian, Design and synthesis of novel N-sulfonyl-2-indoles that behave as 5-HT₆ receptor ligands with significant selectivity for D₃ over D₂ Receptors, *Bioorg. Med. Chem.* 25 (1) (2017) 38–52.
- [13] K. Grychowska, S. Chaumont-Dubel, R. Kurczab, P. Koczurkiewicz, C. Deville, M. Krawczyk, W. Pietruś, G. Satała, S. Buda, K. Piska, et al., Dual 5-HT₆ and D₃ receptor antagonists in a group of 1H-pyrrolo[3,2-c]quinolines with neuro-protective and procognitive activity, *ACS Chem. Neurosci.* 10 (7) (2019) 3183–3196.
- [14] J. Staroń, R. Kurczab, D. Warszycki, G. Satała, M. Krawczyk, R. Bugno, T. Lenda, P. Popik, A.S. Hogendorf, A. Hogendorf, et al., Virtual Screening-Driven Discovery of Dual 5-HT₆/5-HT_{2A} receptor ligands with pro-cognitive properties, *Eur. J. Med. Chem.* 185 (2020), 111857.
- [15] M.J. Millan, A. Dekeyne, A. Gobert, M. Brocco, C. la Cour, J.C. Ortuno, D. Watson, K.C.F. Fone, Dual-acting agents for improving cognition and real-world function in Alzheimer's disease: focus on 5-HT₆ and D₃ receptors as hubs, *Neuropharmacology* (2020), 108099.
- [16] J. Lalut, D. Karila, P. Dallemagne, C. Rochais, Modulating 5-HT₄ and 5-HT₆ receptors in Alzheimer's disease treatment, *Future Med. Chem.* 9 (8) (2017) 781–795.
- [17] D.A. Rodríguez-Soacha, M. Scheiner, M. Decker, Multi-target-directed-ligands acting as enzyme inhibitors and receptor ligands, *Eur. J. Med. Chem.* 180 (2019) 690–706.
- [18] E. Simoni, S. Daniele, G. Bottegoni, D. Pizzirani, M.L. Trincavelli, L. Goldoni, G. Tarozzo, A. Reggiani, C. Martini, D. Piomelli, et al., Combining galantamine and memantine in multitargeted, new chemical entities potentially useful in Alzheimer's disease, *J. Med. Chem.* 55 (22) (2012) 9708–9721.
- [19] M. Incerti, L. Flammini, F. Sacconi, G. Morini, M. Comini, M. Coruzzi, E. Barocelli, V. Ballabeni, S. Bertoni, Dual-acting drugs: an in vitro study of nonimidazole histamine H₃ receptor antagonists combining anticholinesterase activity, *ChemMedChem* 5 (7) (2010) 1143–1149.
- [20] J. Lalut, G. Santoni, D. Karila, C. Lecoutey, A. Davis, F. Nachon, I. Silman, J. Sussman, M. Weik, T. Maurice, et al., Novel multitarget-directed ligands targeting acetylcholinesterase and σ_1 receptors as lead compounds for treatment of Alzheimer's disease: synthesis, evaluation, and structural characterization of their complexes with acetylcholinesterase, *Eur. J. Med. Chem.* 162 (2019) 234–248.
- [21] C. Lecoutey, D. Hedou, T. Freret, P. Giannoni, F. Gaven, M. Since, V. Bouet, C. Ballandonne, S. Corvaisier, A. Malzert Fréon, et al., Design of donecopride, a dual serotonin subtype 4 receptor agonist/acetylcholinesterase inhibitor with potential interest for Alzheimer's disease treatment, *Proc. Natl. Acad. Sci. United States Am.* 111 (36) (2014) E3825–E3830.
- [22] A. Więckowska, M. Kołaczowski, A. Bucki, J. Godyń, M. Marcinkowska, K. Więckowski, P. Zaręba, A. Siwek, G. Kazeł, M. Giuch-Lutwin, et al., Novel multi-target-directed ligands for Alzheimer's disease: combining cholinesterase inhibitors and 5-HT₆ receptor antagonists. design, synthesis and biological evaluation, *Eur. J. Med. Chem.* 124 (2016) 63–81.
- [23] Y.H. Youn, Y.G. Han, Primary cilia in brain development and diseases, *Am. J. Pathol.* 188 (1) (2018) 11–22.
- [24] A.J. Lesiak, M. Brodsky, N. Cohenca, A.G. Croicu, J.F. Neumaier, Restoration of physiological expression of 5-HT₆ Receptor into the primary cilia of null mutant neurons lengthens both primary cilia and dendrites, *Mol. Pharmacol.* 94 (1) (2018) 731–742.
- [25] S.M. Park, H.J. Jang, J.H. Lee, Roles of primary cilia in the developing brain,

- Front. Cell. Neurosci. (2019) 218.
- [26] S. Chaumont-Dubel, V. Dupuy, J. Bockaert, C. Becamel, P. Marin, The 5-HT₆ receptor interactome: new insight in receptor signaling and its impact on brain physiology and pathologies, *Neuropharmacology* (2019), 107839.
- [27] X. Codony, J.M. Vela, M.J. Ramírez, 5-HT₆ receptor and cognition, *Curr. Opin. Pharmacol.* 11 (1) (2011) 94–100.
- [28] I.E.M. de Jong, A. Mørk, Antagonism of the 5-HT₆ Receptor – preclinical rationale for the treatment of Alzheimer's disease, *Neuropharmacology* 125 (2017) 50–63.
- [29] A.V. Ivachtchenko, Y. Lavrovsky, Y.A. Ivanenkov, AVN-211, novel and highly selective 5-HT₆ receptor small molecule antagonist, for the treatment of Alzheimer's disease, *Mol. Pharm.* 13 (3) (2016) 945–963.
- [30] D. Vanda, M. Soural, V. Canale, S. Chaumont-Dubel, G. Satala, T. Kos, P. Funk, V. Fülöpová, B. Lemrová, P. Koczurkiewicz, et al., Novel non-sulfonamide 5-HT₆ receptor partial inverse agonist in a group of imidazo[4,5-b]pyridines with cognition enhancing properties, *Eur. J. Med. Chem.* 144 (2018) 716–729.
- [31] A.S. Hogendorf, A. Hogendorf, R. Kurczab, J. Kalinowska-Tlusćik, P. Popik, A. Nikiforuk, M. Krawczyk, G. Satala, T. Lenda, J. Knutelska, et al., 2-Aminoimidazole-based antagonists of the 5-HT₆ Receptor – a new concept in aminergic GPCR ligand design, *Eur. J. Med. Chem.* 179 (2019) 1–15.
- [32] M.A. Morozova, T.A. Lepilkina, G.E. Rupchev, A.G. Beniashvili, D.S. Burminskiy, S.S. Potanin, E.V. Bondarenko, V.I. Kazey, Y. Lavrovsky, A.V. Ivachtchenko, Add-on clinical effects of selective antagonist of 5-HT₆ receptors AVN-211 (CD-008-0173) in patients with schizophrenia stabilized on antipsychotic treatment: pilot study, *CNS Spectr.* 19 (4) (2014) 316–323.
- [33] S. Schedin-Weiss, M. Inoue, L. Hromádková, Y. Teranishi, N.G. Yamamoto, B. Wiehager, N. Bogdanovic, B. Winblad, A. Sandebring-Matton, S. Frykman, et al., Monoamine oxidase B is elevated in Alzheimer disease neurons, is associated with γ -secretase and regulates neuronal amyloid β -peptide levels, *Alzheimer's Res. Ther.* 9 (1) (2017) 57.
- [34] R.R. Ramsay, Molecular aspects of monoamine oxidase B, *Prog. Neuro-Psychopharmacol. Biol. Psychiatry* 69 (2016) 81–89.
- [35] J.K. Mallajosyula, D. Kaur, S.J. Chinta, S. Rajagopalan, A. Rane, D.G. Nicholls, D.A. Di Monte, H. Macarthur, J.K. Andersen, MAO-B Elevation in mouse brain astrocytes results in Parkinson's pathology, *PLoS One* 3 (2) (2008), e1616.
- [36] J. Saura, J.M. Luque, A.M. Cesura, M. Da Prada, V. Chan-Palay, G. Huber, J. Löffler, J.G. Richards, Increased Monoamine oxidase B activity in plaque-associated astrocytes of Alzheimer brains revealed by quantitative enzyme radioautography, *Neuroscience* 62 (1) (1994) 15–30.
- [37] N.T. Tzvetkov, H.G. Stammer, M.G. Georgieva, D. Russo, I. Faraone, A.A. Balacheva, S. Hristova, A.G. Atanasov, L. Milella, L. Antonov, et al., Carbamides with methanimines: crystal structures, binding interactions, photophysical studies, and biological evaluation of (indazole-5-yl)methanimines as monoamine oxidase B and acetylcholinesterase inhibitors, *Eur. J. Med. Chem.* 179 (2019) 404–422.
- [38] J. Kalinowska-Tlusćik, J. Staroń, A. Krawczuk, S. Mordalski, D. Warszycki, G. Satala, A.S. Hogendorf, A.J. Bojarski, The Effect of the intramolecular C–H...O interactions on the conformational preferences of bis-arylsulfones – 5-HT₆ receptor antagonists and beyond, *RSC Adv.* 8 (33) (2018) 18672–18681.
- [39] W.J. Allen, D.R. Bevan, Steered molecular dynamics simulations reveal important mechanisms in reversible monoamine oxidase B inhibition, *Biochemistry* 50 (29) (2011) 6441–6454.
- [40] C. Binda, F. Hubálek, M. Li, Y. Herzig, J. Sterling, D.E. Edmondson, A. Mattevi, Crystal structures of monoamine oxidase B in complex with four inhibitors of the N-propargylaminoindan class, *J. Med. Chem.* 47 (7) (2004) 1767–1774.
- [41] C. Binda, F. Hubálek, M. Li, Y. Herzig, J. Sterling, D.E. Edmondson, A. Mattevi, Binding of rasagiline-related inhibitors to human monoamine oxidases: a kinetic and crystallographic analysis, *J. Med. Chem.* 48 (26) (2005) 8148–8154.
- [42] T. Tandarić, R. Vianello, Computational insight into the mechanism of the irreversible inhibition of monoamine oxidase enzymes by the anti-parkinsonian propargylamine inhibitors rasagiline and selegiline, *ACS Chem. Neurosci.* 10 (8) (2019) 3532–3542.
- [43] R. Kohen, L.A. Fashingbauer, D.E. Heidmann, C.R. Guthrie, M.W. Hamblin, Cloning of the mouse 5-HT₆ serotonin receptor and mutagenesis studies of the third cytoplasmic loop, *Brain Res. Mol. Brain Res.* 90 (2) (2001) 110–117.
- [44] W. Deraredj Nadim, S. Chaumont-Dubel, F. Madouri, L. Cobret, M.-L. De Tazua, P. Zajdel, H. Benedetti, P. Marin, S. Morisset-Lopez, Physical interaction between neurofibromin and serotonin 5-HT₆ receptor promotes receptor constitutive activity, *Proc. Natl. Acad. Sci. U.S.A.* 113 (43) (2016) 12310–12315.
- [45] K. Grychowska, G. Satala, T. Kos, A. Partyka, E. Colacino, S. Chaumont-Dubel, X. Bantreil, A. Wesolowska, M. Pawlowski, J. Martinez, et al., Novel 1H-pyrrolo [3,2-c]quinoline based 5-HT₆ receptor antagonists with potential application for the treatment of cognitive disorders associated with Alzheimer's Disease, *ACS Chem. Neurosci.* 7 (7) (2016) 972–983.
- [46] F. Duhr, P. Deléris, F. Raynaud, M. Séveno, S. Morisset-Lopez, C. Mannoury La Cour, M.J. Millan, J. Bockaert, P. Marin, S. Chaumont-Dubel, Cdk5 induces Constitutive activation of 5-HT₆ receptors to promote neurite growth, *Nat. Chem. Biol.* 10 (7) (2014) 590–597.
- [47] L. Di, E.H. Kerns, Y. Hong, T.A. Kleintop, O.J. McConnell, D.M. Huryn, Optimization of a higher throughput microsomal stability screening assay for profiling drug discovery candidates, *J. Biomol. Screen* 8 (4) (2003) 453–462.
- [48] B. Liu, A.G. Teschemacher, S. Kasparov, Astroglia as a cellular target for neuroprotection and treatment of neuro-psychiatric disorders, *Glia* 65 (8) (2017) 1205–1226.
- [49] J. Rodriguez-Pallares, J.A. Parga, A. Muñoz, P. Rey, M.J. Guerra, J.L. Labandeira-Garcia, Mechanism of 6-hydroxydopamine neurotoxicity: the role of NADPH oxidase and microglial activation in 6-hydroxydopamine-induced degeneration of dopaminergic neurons, *J. Neurochem.* 103 (1) (2007) 145–156.
- [50] É. Szókó, T. Tábi, P. Riederer, L. Vécsei, K. Magyar, Pharmacological aspects of the neuroprotective effects of irreversible MAO-B inhibitors, selegiline and rasagiline, in Parkinson's disease, *J. Neural. Transm.* 125 (11) (2018) 1735–1749.
- [51] D. Łażewska, R. Kurczab, M. Więcek, K. Kamińska, G. Satala, M. Jastrzębska-Więsek, A. Partyka, A.J. Bojarski, A. Wesolowska, K. Kieć-Kononowicz, et al., The computer-aided discovery of novel family of the 5-HT₆ serotonin receptor ligands among derivatives of 4-benzyl-1,3,5-triazine, *Eur. J. Med. Chem.* 135 (2017) 117–124.
- [52] K. Grychowska, R. Kurczab, P. Śliwa, G. Satala, K. Dubiel, M. Matłoka, R. Moszczyński-Pętkowski, J. Pieczykolan, A.J. Bojarski, P. Zajdel, Pyrroloquinoline scaffold-based 5-HT₆ Ligands: synthesis, quantum chemical and molecular dynamic studies, and influence of nitrogen atom position in the scaffold on affinity, *Bioorg. Med. Chem.* 26 (12) (2018) 3588–3595.
- [53] Glide Version 6.9.
- [54] LigPrep Version 3.6.
- [55] Epik Version 3.4.
- [56] D. Toledo Warshawiak, G. Golan, K.W. Borrelli, K. Zhu, O. Kalid, Structure-based virtual screening approach for discovery of covalently bound ligands, *J. Chem. Inf. Model.* 54 (7) (2014) 1941–1950.
- [57] R. Kurczab, V. Canale, G. Satala, P. Zajdel, A.J. Bojarski, Amino acid hot spots of halogen bonding: a combined theoretical and experimental case study of the 5-HT₇ receptor, *J. Med. Chem.* 61 (19) (2018) 8717–8733.
- [58] A. Partyka, R. Kurczab, V. Canale, G. Satala, K. Marciniak, A. Pasierb, M. Jastrzębska-Więsek, M. Pawlowski, A. Wesolowska, A.J. Bojarski, et al., The impact of the halogen bonding on D₂ and 5-HT_{1A/5-HT₇} receptor activity of azinesulfonamides of 4-[(2-ethyl)piperidinyl-1-yl]phenylpiperazines with antipsychotic and antidepressant properties, *Bioorg. Med. Chem.* 25 (14) (2017) 3638–3648.
- [59] P. Zajdel, T. Kos, K. Marciniak, G. Satala, V. Canale, K. Kamiński, M. Hołuj, T. Lenda, R. Koralewski, M. Bednarski, et al., Novel multi-target azinesulfonamides of cyclic amine derivatives as potential antipsychotics with pro-social and pro-cognitive effects, *Eur. J. Med. Chem.* 145 (2018) 790–804.
- [60] Y. Cheng, W.H. Prusoff, Relationship between the inhibition constant (K_i) and the concentration of inhibitor which causes 50 per cent inhibition (IC_{50}) of an enzymatic reaction, *Biochem. Pharmacol.* 22 (23) (1973) 3099–3108.
- [61] A. Stössel, M. Schlenk, S. Hinz, P. Küppers, J. Heer, M. Gütschow, C.E. Müller, Dual targeting of adenosine A_{2A} receptors and monoamine oxidase B by 4H-3,1-benzothiazin-4-ones, *J. Med. Chem.* 56 (11) (2013) 4580–4596.
- [62] D. Łażewska, A. Olejars-Maciej, D. Reiner, M. Kaleta, G. Latacz, M. Zygmunt, A. Doroz-Pionka, T. Karcz, A. Frank, H. Stark, et al., Dual target ligands with 4-tert-butylphenoxy scaffold as histamine H₃ receptor antagonists and monoamine oxidase B inhibitors, *Int. J. Mol. Sci.* 21 (10) (2020) 3411.
- [63] L.I. Jiang, J. Collins, R. Davis, K.-M. Lin, D. DeCamp, T. Roach, R. Hsueh, R.A. Rebres, E.M. Ross, R. Taussig, et al., Use of a CAMP BRET sensor to characterize a novel regulation of CAMP by the sphingosine 1-phosphate/G13 pathway, *J. Biol. Chem.* 282 (14) (2007) 10576–10584.
- [64] J.K. Singh, S.V. Solanki A, Comparative in vitro intrinsic clearance of imipramine in multiple species liver microsomes: human, rat, mouse and dog, *J. Drug Metabol. Toxicol.* 3 (2012) 126.
- [65] V.N. Sumantran, Cellular chemosensitivity assays: an overview, *Methods Mol. Biol.* 731 (2011) 219–236.
- [66] A. Ennaceur, J. Delacour, A new one-trial test for neurobiological studies of memory in rats. 1: behavioral data, *Behav. Brain Res.* 31 (1) (1988) 47–59.
- [67] P. Popik, M. Holuj, A. Nikiforuk, T. Kos, R. Trullas, P. Skolnick, 1-Aminocyclopropanecarboxylic acid (ACPC) produces procognitive but not antipsychotic-like effects in rats, *Psychopharmacology* 232 (6) (2015) 1025–1038.